ChemPubSoc Europe

DOI: 10.1002/chem.201903644

CHEMISTRY A European Journal Full Paper

Photochemistry

Improving the Switching Capacity of Glyco-Self-Assembled Monolayers on Au(111)

Ellen Fast[+],[a] Alexander Schlimm[+],[b] Irene Lautenschläger,[b] Kai Uwe Clausen,[b] Thomas Strunskus,[c] Carina Spormann,[a] Thisbe K. Lindhorst,*[a] and Felix Tuczek*[b]

Abstract: Self-assembled monolayers (SAMs) decorated with photoisomerizable azobenzene glycosides are useful tools for investigating the effect of ligand orientation on carbohydrate recognition. However, photoswitching of SAMs between two specific states is characterized by a limited capacity. The goal of this study is the improvement of photoswitchable azobenzene glyco-SAMs. Different concepts, in particular self-dilution and rigid biaryl backbones, have been investigated. The required SH-functionalized azobenzene glycoconjugates were synthesized through a modular approach, and the respective glyco-SAMs were fabricated on Au(111). Their photoswitching properties have been extensively investigated by applying a powerful set of methods (IRRAS, XPS, and NEXAFS). Indeed, the combination of tailor-made biaryl-azobenzene glycosides and suitable diluent molecules led to photoswitchable glyco-SAMs with a significantly enhanced and unprecedented switching capacity.

Introduction

Many biological processes, such as cell signaling, cell recognition, and cell adhesion, are mediated by molecular interactions occurring at the cell surface, which is covered by a layer of diverse glycoconjugates, called the glycocalyx.[1] Therefore, elucidation of the mechanisms that underpin carbohydrate recognition is key to our understanding of cell surface biology. Carbohydrates are ligands of a class of proteins called lectins,[2] which apparently govern most cell–cell interactions through specific carbohydrate–lectin interactions. For example, many *Enterobacteriaceae*, such as *Escherichia coli* (*E. coli*), accomplish firm adhesion to the surface of their host cells through lectins, which are constituents of adhesive organelles projecting from the bacterial surface called fimbriae (or pili).[3] Among the most important bacterial fimbriae are so-called type 1 fimbriae, which mediate adhesion to terminal α-D-mannopyranoside components of the glycocalyx through the type 1-fimbrial lectin FimH.[4]

Many principles of the highly complex supramolecular interactions leading to cell adhesion are still not well understood. Therefore, model systems, in particular so-called glyco-SAMs (self-assembled monolayers),[5] have been used to mimic the glycocalyx and to allow the investigation and interrogation of carbohydrate–protein interactions on surfaces. As a first step in this direction, we prepared glyco-SAMs derived from molecules composed of an azobenzene moiety, an alkanethiol linker, and a mannoside head group, and investigated them by X-ray photoelectron spectroscopy (XPS), near-edge X-ray absorption fine structure (NEXAFS), and infrared reflection-absorption spectroscopy (IRRAS).[6] Here, photoisomerization of the azobenzene N=N double bond between two isomeric states (*trans* and *cis*) allows the reversible reorientation of a sugar ligand, if the molecule is properly adsorbed on a surface. Indeed, when conjugated to an alkanethiol chain, azobenzene glycosides self-assemble into monolayers on gold (Au(111)). Utilizing the intensity change of the C(aryl)–O(mannoside) IR stretching band upon *cis*/*trans* isomerization (*E*/*Z* isomerization), we were able to monitor a reversible, photoinduced switching of the orientation of the head group. Nevertheless, the observed intensity change was small (about 4%). More recently, we showed the importance of ligand orientation in carbohydrate-specific bacterial adhesion using an SAM of azobenzene glycosides containing oligoethylene (OEG) moieties.[7] When we applied this system to bacterial adhesion, the adhesion of type 1 fimbriated *E. coli* was found to be greatly reduced in the *cis* form as compared to the *trans* form. Remarkably, photoswitching of

[a] E. Fast,[+] C. Spormann, Prof. Dr. T. K. Lindhorst
Otto Diels Institute of Organic Chemistry, Christian-Albrechts-University Kiel
Otto-Hahn-Platz 4, 24118 Kiel (Germany)
E-mail: tklind@oc.uni-kiel.de

[b] Dr. A. Schlimm,[+] I. Lautenschläger, K. U. Clausen, Prof. Dr. F. Tuczek
Institute of Inorganic Chemistry, Christian-Albrechts-University Kiel
Max-Eyth Straße 2, 24118 Kiel (Germany)
E-mail: ftuczek@ac.uni-kiel.de

[c] Dr. T. Strunskus
Institute for Materials Science—Multicomponent Materials
Christian-Albrechts-University Kiel, Kaisertr. 2, 24143 Kiel (Germany)

[+] These authors contributed equally to this work.

Supporting information and the ORCID identification number(s) for the author(s) of this article can be found under: https://doi.org/10.1002/chem.201903644.

azobenzene glycoconjugates also alters bacterial adhesion on cell surfaces.[8]

Regarding the actual performance of photoswitchable glyco-SAMs, it is important to note that the *trans-cis* isomerization of the azobenzene moiety is associated with a large spatial change and, therefore, the molecules on the surface require enough free volume to undergo the process. This, however, is in direct conflict with the nature of most SAMs, which consist of densely packed molecules.[9] Accordingly, in our first study employing glycoazobenzene alkanethiols without an OEG group, less bulky alkanethiols were needed as diluent molecules to achieve *trans-cis* isomerization of the glycoazobenzenes in SAMs (Figure 1 a).[6] On the other hand, when we switched to bacterial adhesion, the employed SAMs containing OEG moieties and no further diluent molecules could be used for the fabrication of photoswitchable SAMs.[7] The precise influence of the OEG groups on the switching properties of the respective glyco-SAMs is unclear.

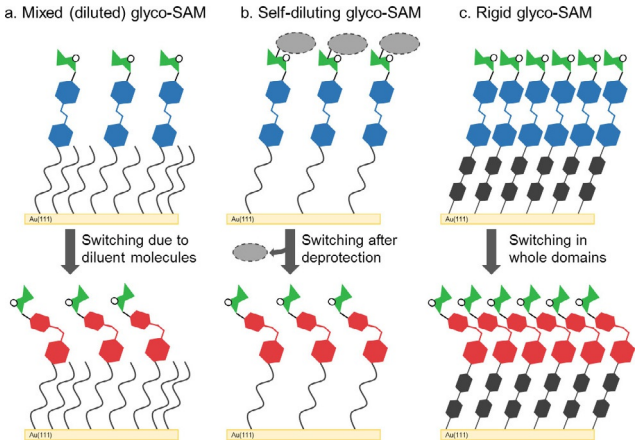

Figure 1. Three different approaches for fabricating photoswitchable glyco-SAMs from azobenzene glycoconjugates: a) *cis-trans* isomerization is facilitated by diluent molecules; b) concept of self-dilution; c) photoswitching of rigid (biphenyl-containing) SAMs. The *trans* (*E*)-state of the azobenzene hinge is shown in blue, the *cis* (*Z*)-state in red, the green sugar residue symbolizes α-D-mannopyranoside, and the grey oval a bulky protecting group.

In order to further improve the properties of photoswitchable glyco-SAMs, it is essential to understand the dependence of the switching capacity (i.e., the fraction of molecules undergoing photoinduced *cis/trans* isomerization) on the physicochemical properties of the head groups and the underlying SAM. Key parameters in this regard are the rigidity of the chains incorporated into the molecules forming the SAM, their lateral density, as well as their intermolecular interactions, and the free volume required for the switching of the head groups.[10,11] A first approach to providing sufficient free volume for photoswitching was based on the application of nonplanar substrates such as nanoparticles. Because of the surface curvature of these particles, the adsorbed molecules have significantly more free volume than those on a flat surface.[10,12] Other concepts also permit effective photoisomerization on flat surfaces, such as the platform approach,[13,14] whereby the size of a ring system adsorbed on a gold surface determines the intermolecular distances of the photoswitchable molecules mounted on this platform. This approach can be turned upside down by using bulky protecting groups, which provide space between the chemisorbed molecules during SAM formation and can be cleaved on the surface after the adsorption process. Lahann et al. showed that such SAMs are stable even after the deprotection step.[15] This approach can be termed a self-diluting process (Figure 1 b). On the contrary, SAMs can also be fabricated from molecules based on rigid biphenyl backbones, leading to especially densely packed monolayers due to strong intermolecular π–π interactions (Figure 1 c). Counterintuitively, such SAMs, consisting of azobenzene-biphenyl thiols, for example, show excellent switching properties on surfaces.[16] Pace et al. attributed these results to a cooperative character of the switching process.[16]

Herein, we adapt both of these approaches towards effective photoisomerization of azobenzene-containing SAMs (that is, combining Figure 1 b, c)[15,16] in the design of new azobenzene glyco-SAMs, with a view to achieving improved switching behavior. Because of its biological importance, azobenzene α-D-mannoside was selected as the photoswitchable carbohydrate ligand, as in our earlier work.[6,7] Regarding the self-diluting approach, the 6-position of the mannopyranoside ring offers an ideal attachment point for a bulky protecting group. For the fabrication of rigid SAMs, aryl-aryl cross-coupling reactions were employed to conjugate azobenzene α-D-mannoside to a rigid backbone. The chemical composition and integrity of the prepared SAMs were determined by XPS, and their switching capacities were investigated using a combination of IRRAS and NEXAFS.

Results and Discussion

Synthesis

For the fabrication of self-diluting SAMs (see Figure 1 b), glycoazobenzene alkanethiols were required, bearing a bulky protecting group that can be cleaved under mild conditions on the SAM surface. The primary hydroxy group of the sugar moiety is a practical position for the installation of a bulky moiety as it is amenable to regioselective reaction. In first attempts, a trityl group was selected for modification at the 6-OH, but this caused problems in later steps of the synthesis. Then, a *tert*-butyldiphenylsilyl (TBDPS) ether was evaluated for protection of the 6-position of the sugar, which could be cleaved under mild acidic conditions or by fluoride ions. This approach worked very well, even with free D-mannose, whereby regioselective silylation of the 6-hydroxy group followed by protection of the secondary OH groups by acetylation furnished the mannose tetraacetate **2** in 74% yield over two steps (Scheme 1). This derivative was then converted into a mannosyl donor, the route entailing initial selective deprotection of the anomeric position by employing ethylenediamine in a mixture with acetic acid,[17] followed by base-promoted addition of the reducing sugar **3** to trichloroacetonitrile to yield

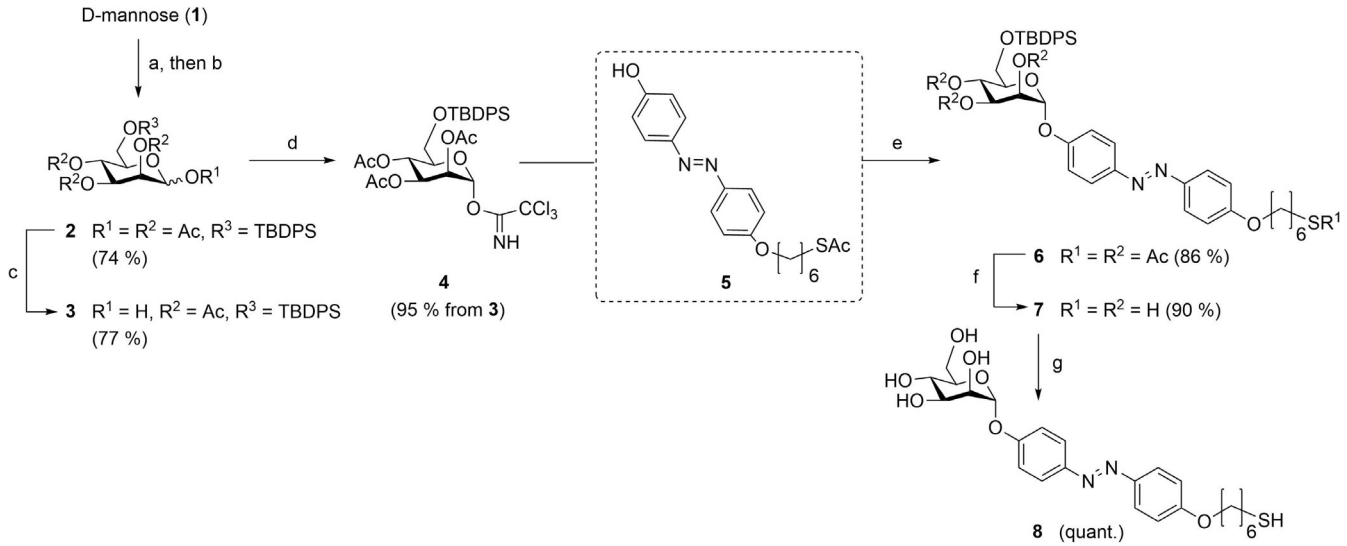

Scheme 1. Synthesis of the 6-*O*-silylated mannoside **7** for fabrication of self-diluting glyco-SAMs. Reagents and conditions: a) TBDPS-Cl, DMAP, pyridine, 16 h, rt; b) Ac_2O, pyridine, 16 h, rt; c) $H_2N(CH_2)_2NH_2$, H_3CCO_2H, THF, rt, 16 h; d) Cl_3CCN, DBU, CH_2Cl_2, 0 °C→rt, 2 h; e) $BF_3{\cdot}OEt_2$, CH_2Cl_2, 0 °C→rt, 2 h; f) MeOH, NaOMe, rt, 1 h; g) THF, TBAF, 4 h rt. TBDPS: *tert*-butyldiphenylsilyl; DMAP: 4-dimethylaminopyridine; DBU: 1,8-diazabicyclo[5.4.0]undec-7-ene; TBAF: tetrabutylammonium fluoride.

the *O*-mannosyl trichloroacetimidate **4**,[18] bearing the requisite bulky protecting group at C-6.

In the following mannosylation step, the hydroxy azobenzene derivative **5** served as glycosyl acceptor. It bears the aliphatic 6-acetylthio-hexanyl linker, which is required for the fabrication of SAMs. It was obtained by selective nucleophilic substitution of 6-acetylthio-1-hexanesulfonate with dihydroxyazobenzene (see the Supporting Information). The Lewis-acid-promoted reaction of **4** with **5** under standard conditions[19] gave the desired mannoside **6** in excellent yield, exclusively as the α-anomer. Treatment of the protected mannoside **6** with sodium methanolate in methanol to liberate both the OH groups and the thiol group gave **7** in 90% yield. When this thiol was freshly prepared as for the fabrication of SAMs, no disulfide oxidation products were present according to NMR and MS analyses. To test the feasibility of the silyl ether cleavage, **7** was submitted to standard deprotection conditions using TBAF (Scheme 1) to quantitatively deliver the OH-free mannoside **8** (for ^{1}H NMR data, see the Supporting Information).

In view of the high yields and selectivities of the described reactions, the thiohexyl-modified azobenzene mannoside **7** appears to be an ideal molecule for testing the concept of self-dilution to facilitate photoisomerization of SAMs (see below).

For the fabrication of rigid SAMs, the molecules depicted in Figure 2 were targeted. The two mannosides differ in the arrangement of the biphenyl and azo moieties relative to the sugar head group. A third azobenzene derivative was required, that is, a less bulky yet still photoswitchable diluent molecule (see below). Figure 2 exemplifies the modular synthetic approach employed, where in each case complementary aryl iodides and arylboronic esters could be cross-coupled in a Suzuki reaction.[20] Furthermore, it was necessary to select an appropriate method to furnish the free arylthiol functional groups. It was found that the Newman–Kwart rearrangement

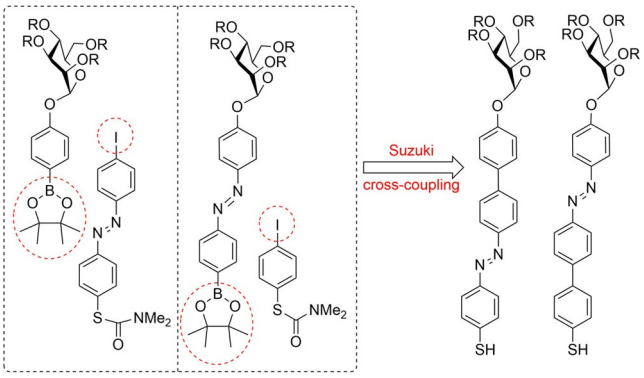

Figure 2. A modular synthesis delivers the target molecules (right) for the fabrication of rigid SAMs, employing the respective aryl iodides and arylboronic esters (boxed on the left) in Suzuki cross-coupling. *S*-Thiocarbamates were derived from the respective *O*-thiocarbamates by Newman–Kwart rearrangement and served as precursors of the required aromatic thiols.

could be successfully employed, in which *O*-thiocarbamates are thermally rearranged to *S*-thiocarbamates by intramolecular aryl migration. The latter can be readily hydrolyzed under basic conditions to deliver the required thiophenols.

The photoswitchable mannoside **14** (Scheme 2) was selected as a first target molecule for the rigid SAM approach. For its synthesis, commercially available iodo hydroxyazobenzene **9** was reacted with dimethylthiocarbamoyl chloride and DABCO as a non-nucleophilic base to give **10** in a very good 82% yield. In the following Newman–Kwart rearrangement, the *S*-thiocarbamate **11** was formed under solvent-free conditions at 200 °C in almost quantitative yield (97%).

In the penultimate step of the synthesis, the iodoazobenzene **11** was subjected to a Suzuki coupling with the literature-known boronic ester **12**[21] in order to introduce the α-D-

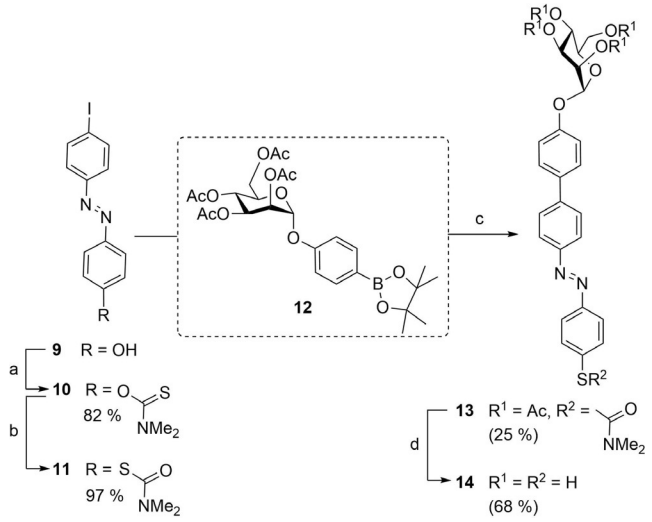

Scheme 2. Synthesis of the rigid *p*-mannosyloxyphenyl-azobenzene derivative **14**. Reagents and conditions: a) DABCO, dimethylthiocarbamoyl chloride, DMF, 5 h, 70 °C; b) 200 °C, 3 h; c) K_2CO_3, TBABr, $Pd(PPh_3)_4$, toluene, H_2O, 4 h, 80 °C; d) KOH, MeOH, 16 h, rt. DABCO: 1,4-diazabicyclo[2.2.2]octane; TBABr: tetrabutylammonium bromide.

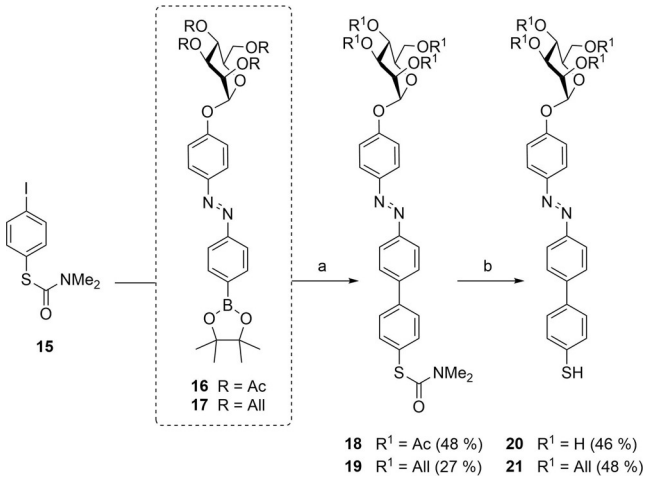

Scheme 3. Synthesis of the rigid *p*-mannosyloxy-*p*′-phenylazobenzene derivatives **20** and **21**. Reagents and conditions: a) $Pd(PPh_3)_4$, K_2CO_3, TBABr, toluene, H_2O, 16 h, 90 °C; b) KOH, MeOH, 1–2 h, reflux. TBABr: tetrabutylammonium bromide.

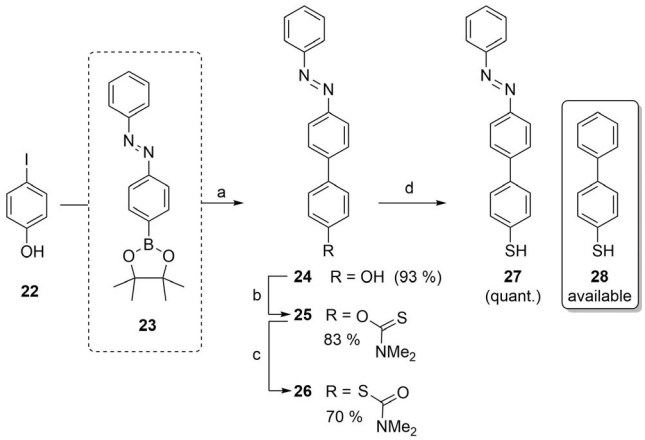

Scheme 4. Diluent molecules **27** and **28** for the fabrication of mixed SAMs. Reagents and conditions for the synthesis of **27**: a) bis(2-amino-4,6-dihydroxypyrimidine)palladium(II) diacetate, MeOH, Na_2HPO_4, 2 h, 60 °C; b) NaH, dimethylthiocarbamoyl chloride, DMF, 24 h, 98 °C, c) 270 °C, 15 min; d) KOH, MeOH, 2 h 70 °C.

mannopyranoside head group. This palladium-catalyzed reaction was performed in a biphasic solvent mixture with tetrabutylammonium bromide (TBABr) as phase-transfer catalyst and delivered the protected mannoside **13** in a moderate yield of 32%. The final deprotection step under basic conditions removed the *O*-acetyl protecting groups and concomitantly delivered the free arylthiol to furnish the target molecule **14**.

As an alternative to **14**, having a biphenyl spacer "above" the N=N group, mannoside **20** was synthesized, in which the biphenyl spacer is positioned "below" the N=N moiety. To this end, the *S*-thiocarbamate **15**[22] and the mannosyloxyazobenzeneboronate ester **16** or **17**, respectively, were submitted to the Suzuki reaction to yield the desired cross-coupling products, **18** and **19**, respectively, in moderate yields. The boronates bearing different sugar protecting groups were obtained from the respective literature-known aryl iodides in high yields (see the Supporting Information). Our chosen synthetic route provides advantageous flexibility with respect to variation of the sugar head group.

The Newman–Kwart rearrangement delivered the target mannoside **20** bearing the free arylthiol group starting from the *O*-acetylated analogue **18**. Subjecting the *O*-allylated derivative **19** to the same reaction conditions gave **21** (Scheme 3). We were interested in investigating the influence of the sugar protecting groups on the photoswitchability of SAMS fabricated from these molecules. The OH-unprotected mannosides are rather hydrophilic in comparison to their protected analogues, and *O*-acetylation leads to more electron-deficient glycosides as opposed to their *O*-allylated analogues.

In order to modify SAMs formed from the *p*-mannosyloxy-*p*′-phenyl-azobenzene derivative **20** as mixed SAMs, the azobenzene derivative **27** was prepared as a photoswitchable diluent molecule (Scheme 4). When incorporated into SAMs, it can provide space for the mannose head groups, while also engaging in π–π interactions in the backbone of the SAM. Because we were not satisfied with the yields obtained from the Suzuki cross-coupling reactions, we tried various catalysts to improve the yields of this coupling. For the synthesis of **24**, bis(2-amino-4,6-dihydroxypyrimidine)palladium(II) diacetate was synthesized from palladium acetate[23] and used for the coupling of **22** and **23**.[24] Indeed, this gave the biphenyl azobenzene **24** almost quantitatively.[25]

Unfortunately, the same catalyst and reaction conditions did not lead to improvement of the yields for the mannoside analogues (see Schemes 2 and 3). Reaction of **24** with dimethylthiocarbamoyl chloride and sodium hydride gave the *O*-thiocarbamate **25**, subsequent heating of which for 15 min at 270 °C in a Kugelrohr distillation apparatus gave the rearranged *S*-thiocarbamate **26** in good yield. In this case, the rear-

rangement step had to be carefully controlled as longer reaction times resulted in low yields or even decomposition. As before, the free SH group was furnished by treatment with an excess of KOH to give the diluent molecule **27**, which could then be compared with commercially available 4-biphenylthiol (**28**) (see below).

Prior to SAM fabrication and investigation of their photoswitchability, the switching properties of the synthesized compounds were investigated in homogeneous solution (see the Supporting Information). The photostationary states (PSS) and the half-lives associated with the thermal *cis-trans* relaxation were determined by NMR spectroscopy (see Table S12). As the investigated azobenzene derivatives are soluble in different solvents, the comparability of the results is somewhat limited, but clearly all of the tested compounds, **7**, **8**, **14**, **20**, **21**, and **27**, can be reversibly photoswitched between their *cis* and *trans* forms in homogeneous solution. The determined half-lives of thermal *cis*→*trans* relaxation are in the usual range (12–15 h), with the exception of those of **20** and **27**, which exhibit faster *cis*→*trans* relaxation (half-lives <2 h).

Surface spectroscopic investigation of the self-diluting glyco-SAMs

First, the concept of self-diluting SAMs was evaluated. To this end, the azobenzene mannoside **7** bearing the bulky TBDPS protecting group at C-6 was employed. An SAM of this molecule was deposited on Au(111) by immersing a gold substrate in a solution of **7** in methanol. The resulting monolayer was investigated by means of a range of surface-spectroscopic and surface-analytical methods. For comparison, an SAM of the azobenzene mannoside **8**, the deprotected analogue of **7**, was also prepared and investigated by the same methods.

X-ray photoelectron spectroscopy and near-edge X-ray absorption fine structure spectroscopy

In order to check the integrity and purity of the adsorbed molecular layer of **7**, X-ray photoelectron spectroscopy (XPS) was employed. The resulting spectra are shown in Figure 3. The C 1s region contains four different signals (Figure 3a). The main component at 284.7 eV (red) corresponds to the carbon atoms bound to other carbon, hydrogen, silicon, and sulfur atoms. The second species (blue) at 285.3 eV is associated with carbon atoms bound to nitrogen atoms. The signals at higher binding energies (286.4 and 288.0 eV) correspond to carbon atoms bound to oxygen. Of these, the signal shown in green is assigned to the carbon atoms bound to only one oxygen atom, and the signal in orange to the anomeric carbon atom bound to two oxygen atoms. Importantly, the relative contributions of the different species fit exactly to the ratio (75:5:18:2) derived from the chemical composition of the azobenzene mannoside.

In the N 1s region, only one signal at 399.5 eV is observed, which corresponds to the nitrogen atoms of the azo group (Figure 3b).[6,26,27] The S 2p region, on the other hand, shows a doublet at 161.9 and 163.1 eV (Figure 3c). The binding energy

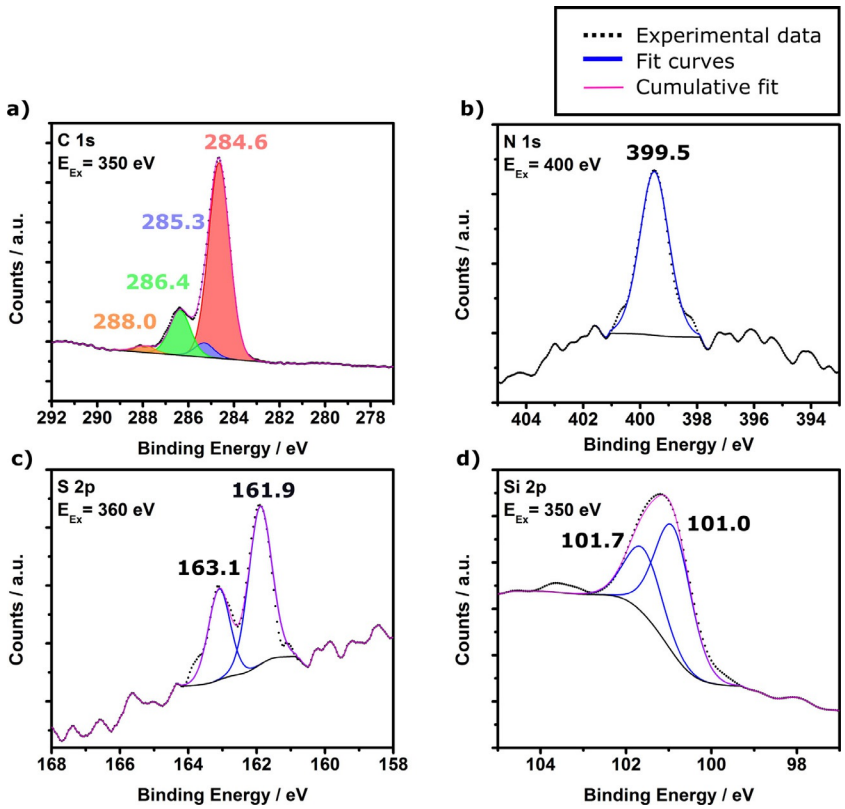

Figure 3. X-ray photoelectron spectroscopy data of compound **7** adsorbed on Au(111). Four different regions are shown: C 1s (a), N 1s (b), S 2p (c), and Si 2p (d).

and the splitting of 1.2 eV are characteristic of a thiolate moiety.[28–30] The presence of this species proves the covalent attachment of the molecules to the gold surface. The Si 2p region also features one doublet (101.0 and 101.7 eV), which can be assigned to the silicon atom of the protecting group (Figure 3 d).

Further information on the constitution of the SAM of **7** on Au(111) was provided by NEXAFS recorded at the carbon and nitrogen K-edges (see the Supporting Information, Figure S6). The nitrogen K-edge NEXAFS shows a characteristic resonance at 399.1 eV. The energy of this feature corresponds well to the N 1s-to-π* transition reported in the literature for azobenzene units.[27] Angle-dependent measurements (Supporting Information, Figure S6) show that the intensity of this resonance increases from the 30° the 90° spectrum. This allows determination of the orientation of the molecule on the surface.[27]

The tilt angle α of the N 1s-to-π* transition dipole moment relative to the surface normal was determined as $58\pm2^\circ$. Since this transition dipole moment is perpendicular to the molecular axis for *trans*-azobenzene, the azobenzene shows a molecular tilt angle β of $32\pm2^\circ$ with respect to the surface normal ($90^\circ-\alpha=\beta$; see Figure 4). This is in good agreement with the tilt angles of other alkyl-SAMs reported in the literature.[31] The carbon K-edge NEXAFS features several resonances. The most prominent π* resonance at 285.5 eV shows a weak angular dependence, its intensity decreasing at lower angles of incidence. This result is in accordance with the N-NEXAFS data (see the Supporting Information, Figure S6).

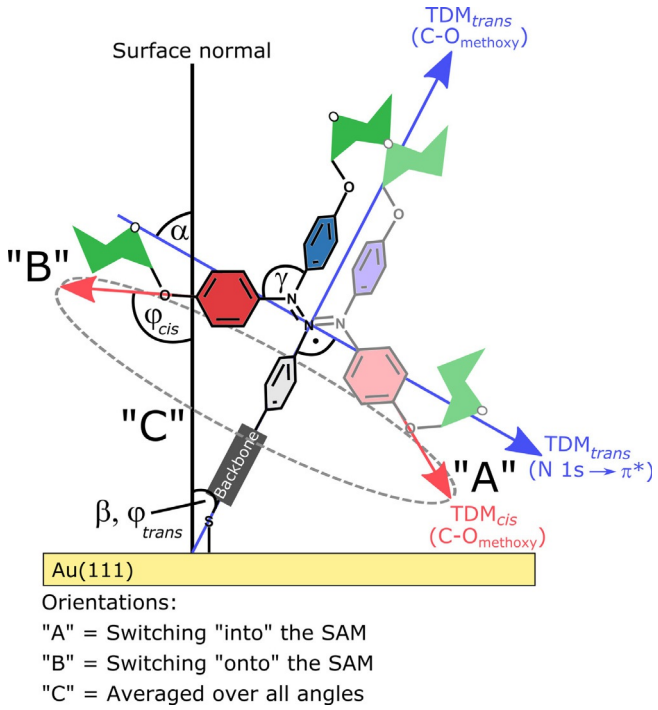

Figure 4. Definition of the NEXAFS and IRRAS transition dipole moments (TDM) and angles for the determination of molecular orientation. The two different orientations A and B of the TDM of the C_{aryl}–O stretching vibration in the *cis* isomer are shown. The average over all angles of the rotation about the molecule axis is referred to as orientation C.

Infrared reflection absorption spectroscopy

The SAM of **7** (Figure 5 a) and its switching behavior were further investigated by means of infrared reflection absorption spectroscopy (IRRAS). Intensities of around 10^{-3} absorbance units are compatible with the formation of a monolayer on Au(111) (Figure 5 c).[14] Notably, the different relative intensities in the measured bulk and surface IR spectra, in particular in the regions around 1600 and 1200 cm^{-1}, are caused by the surface selection rule.[32] Such differences give a first indication of a well-organized monolayer and a preferred orientation of the molecules on the surface.

The measured IR spectra were compared to calculated bulk IR spectra in order to assign the bands to specific vibrational modes. The IRRA spectrum of **7-SAM** features several significant bands in the fingerprint region. The bands around 1600 cm^{-1} correspond to C_{aryl}–C_{aryl} stretching vibrations of the azobenzene unit. A combination of the N=N stretching and aromatic C–C stretching vibrations is seen at 1498 cm^{-1}. The most prominent vibration at 1247 cm^{-1} can be assigned to the C_{aryl}–O stretching vibration of the glycosidic oxygen. Importantly, the transition dipole moment of this vibrational mode is parallel to the axis of the azobenzene unit in the *trans* state, thus showing the same orientation with respect to surface normal as the azobenzene unit in the SAM. Moreover, the orientation of this vibration changes during isomerization of the azobenzene N=N double bond. This, in turn, directly influences the intensity of the band in the surface IR spectrum because of the surface selection rule.[32] The C_{aryl}–O vibration is thus well suited for monitoring the *cis*/*trans* isomerization of the glyco-SAMs adsorbed on Au(111) through IRRAS.[6]

In order to detect the isomerization process with high sensitivity, PM-IRRAS (polarization-modulated IRRAS) in the spectral range of the C_{aryl}–O vibration was applied. Due to the presence of a small shoulder in the investigated IR band (C_{aryl}–O stretching vibration) at lower wavenumbers, the band was fitted with two Gaussians to determine the intensity of the pure C_{aryl}–O band (see the Supporting Information, Figures S14–S19). The second band corresponds to a C–H bending vibration within the mannose moiety. This vibration is a combination of different vibrational modes. Moreover, the mannose moiety can rotate about the anomeric C–O bond. For this reason, the intensity of this band is barely affected by the isomerization process and can be considered as constant. The change in the C_{aryl}–O bond orientation was calculated by geometry optimizations of the *cis* and *trans* isomers (see the Supporting Information, Figure S22). For the *cis* isomer, a CNNC angle (C_{aryl}–N_{azo}=N_{azo}–C_{aryl}) of 69.4° was obtained, as compared to 179.9° for the *trans* isomer. Thus, the CNNC angle change (γ) amounts to 110.5° during the isomerization reaction (see Figure 4), in good agreement with data on pure azobenzenes reported in the literature.[33] Nevertheless, only small changes ($\Delta I_{exp}=2\%$) of the C_{aryl}–O stretching intensity were observed upon irradiation of **7-SAM** adsorbed on gold with light of 365 nm (Figure 5 d; see the Supporting Information, Figure S16).

Utilizing the tilt angle β determined by NEXAFS, the angle ϕ between the transition dipole moment of the C_{aryl}–O stretch-

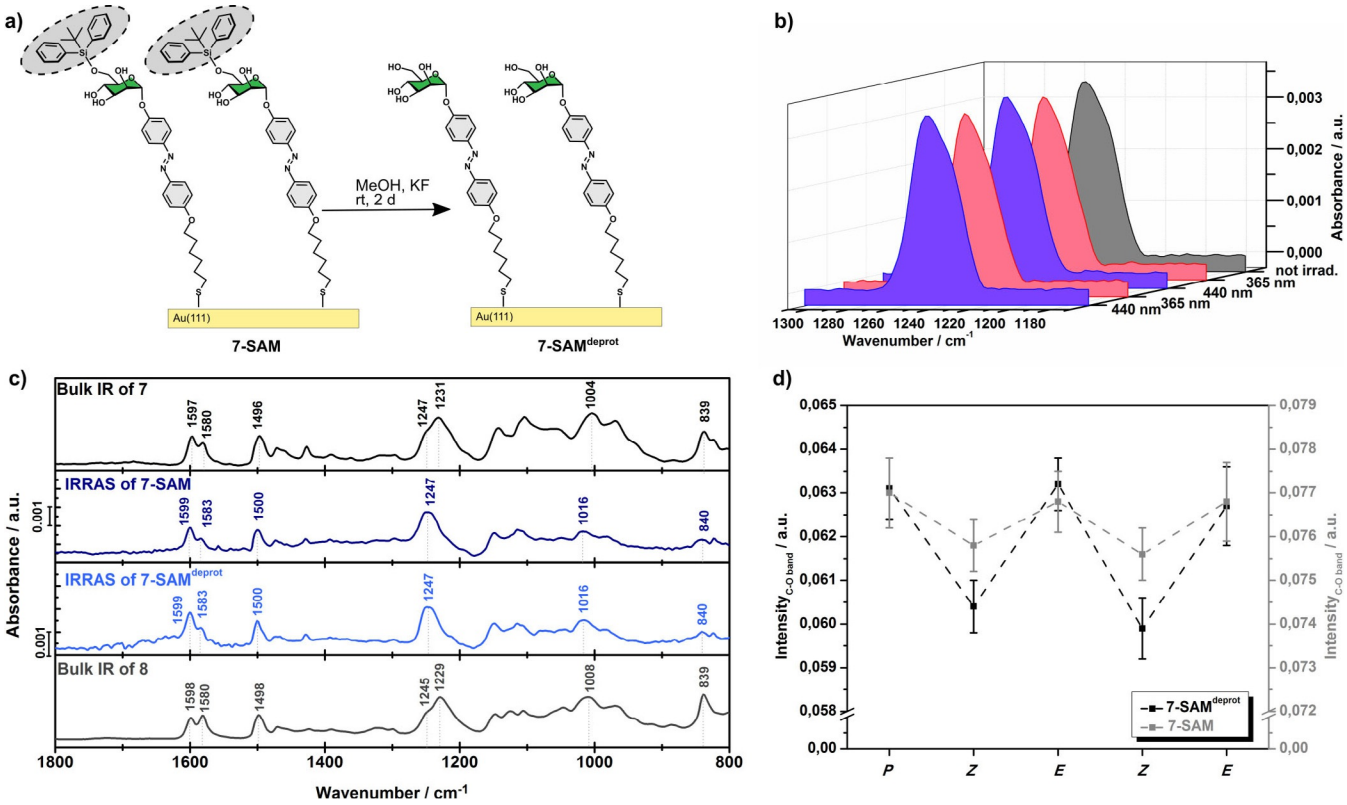

Figure 5. Vibrational data for compounds **7** and **8**. a) Deprotection of the **7-SAM** with KF leads to the **7-SAM^{deprot}**. b) This display shows the reversibility of the *cis*/*trans* isomerization of the **7-SAM^{deprot}** by means of the C_{aryl}—O stretching intensity after irradiation with light of 365 nm or 440 nm. c) The measured bulk IR spectra of compound **7** before and after deprotection (**8**) and the IRRA spectra of compound **7** in a monolayer on Au(111) before and after cleavage of the TBDPS group (**7-SAM^{deprot}**). d) Comparison of the switching behavior before (**7-SAM**, gray) and after (**7-SAM^{deprot}**, black) cleavage of the TBDPS group.

ing vibration and the surface normal can be determined. However, whereas for the *trans* form $\phi_{trans}=\beta$, there are several possibilities for the *cis* form, that is, the azo group can isomerize towards the surface ("into" the SAM, A) or into a configuration more parallel to the surface ("onto" the SAM, B; $\phi(A)_{cis}=180^\circ-\gamma-\beta$, $\phi(B)_{cis}=\gamma-\beta$; Figure 4). Moreover, an equal distribution of all transition dipole orientations within these two extremes, that is, within a corresponding cone around the molecular axis, is theoretically possible (Figure 4c). In this case, a rotational averaging over all possible azimuthal angles has to be performed (see the Experimental Section). Although, due to steric reasons, there may be a preferential orientation of the head group (e.g., B) in the *cis* configuration of the investigated glyco-SAMs, this issue cannot be resolved without further information. In view of this situation, in Table 1 we compare ΔI_{exp} values based on IRRAS data with ΔI_{theo} values obtained for orientations A (head group towards the surface), B (head group approximately parallel to the surface), and C (rotational

Table 1. Comparison of the switching behavior of the investigated glyco-SAMs.[a]

SAM	Tilt angle (β)	ϕ $(A)_{cis}$	ϕ $(B)_{cis}$	ΔI_{theo} A[b]	ΔI_{theo} B[c]	ΔI_{theo} C[d]	ΔI_{exp}[e]	$\Delta I_{exp}/\Delta I_{theo}$[f]	Reversibility
7-SAM	$32\pm2^\circ$	$38\pm2^\circ$	$79\pm2^\circ$	14%	94%	71%	2%	3%	yes
7-SAM^{deprot}[g]	$33\pm2^\circ$	$37\pm2^\circ$	$78\pm2^\circ$	11%	94%	69%	5%	7%	yes
8-SAM	–	–	–	–	–	–	<1%	–	–
20-SAM	$23\pm6^\circ$	$47\pm6^\circ$	$88\pm6^\circ$	45%	99%	80%	27%	34%	no
20,27-SAM	$22\pm2^\circ$	$48\pm2^\circ$	$89\pm2^\circ$	47%	99%	80%	38%	48%	yes
20,28-SAM	$24\pm3^\circ$	$45\pm3^\circ$	$87\pm3^\circ$	41%	99%	78%	18%	23%	yes
21-SAM	$24\pm5^\circ$	$45\pm5^\circ$	$87\pm5^\circ$	41%	99%	78%	9%	12%	yes
14-SAM	$29\pm3^\circ$	$40\pm3^\circ$	$81\pm3^\circ$	24%	97%	73%	5%	7%	no

[a] β is the tilt angle with respect to the surface normal. The angle ϕ describes the orientation of the transition dipole moment of the C—O_{aryl} stretching vibration in the *cis* isomer with respect to the surface normal. A and B describe the two extrema from Figure 4. The value ΔI_{theo} corresponds to the expected maximum intensity change of the C—O_{aryl} stretching vibration considering β and the spatial change during the isomerization in dependence on the orientation of the *cis* isomer within the glyco-SAM (A: head group downwards; B: head group upwards; C: average). [b] Based on orientation A. [c] Based on orientation B. [d] Based on averaged orientation C. [e] Experimentally (IRRAS) obtained intensity change. [f] Switching capacity based on C. [g] Superscript "deprot" denotes on-surface cleavage of the TBDPS group.

average). Based on C, an intensity decrease of $\Delta I_{theo} = 71\%$ is predicted if all molecules in the **7-SAM** switch to the *cis* isomer. The observed intensity change ($\Delta I_{exp} = 2\%$) would thus indicate that only 3% of the molecules switch to the *cis* isomer (Table 1). Taking the steric demand of the TBDPS group into account, this result is consistent with previous studies[6] on pure glyco-SAMs.

In order to increase the free volume for the *trans*→*cis* isomerization of surface-adsorbed compound **7**, the protecting group was cleaved off by immersing the functionalized substrate in a solution of potassium fluoride in methanol for 2 days (Figure 5a). The resulting **7-SAM^{deprot}** (after on-surface cleavage of the TBDPS group) was again investigated by XPS, NEXAFS, and IRRAS to evaluate its switching behavior. Except for small changes in intensity, the surface IR spectrum, shown in Figure 5c, exhibited no significant differences between the protected and deprotected SAMs of compound **7** on Au(111). This result is consistent with the similarity of the bulk spectrum of **7** and the bulk spectrum of **8** obtained by deprotection of **7** in homogeneous solution (Figure 5c).

In contrast to the vibrational spectra, the XPS data (see the Supporting Information, Figure S1) clearly reflect the successful deprotection reaction on the surface, with the signal in the Si 2p region becoming significantly weaker. These data suggest that most of the TBDPS groups were in fact cleaved by treatment of the functionalized substrate with potassium fluoride. At the same time, the SAM stayed intact according to the S 2p spectrum, which, even after on-SAM deprotection (see the Supporting Information, Figure S1), still prominently featured the peaks of the thiolate species. The orientation of **7-SAM^{deprot}** was again elucidated by NEXAFS. Remarkably, after the on-surface deprotection, the tilt angle β was still $33 \pm 2^\circ$ ($\Delta I_{theo} = 69\%$, based on orientation C), very similar to the original value (see the Supporting Information, Figure S12). This underscores the conformational stability of **7-SAM**, which maintains its original orientation even after cleavage of its TBDPS groups.

After deprotection, the intensity change due to the *trans*/*cis* isomerization increased significantly ($\Delta I_{exp} = 5\%$; Figure 5b, d). Based on the rotationally averaged *cis* configuration C, this intensity change indicates that 7% of the molecules on the surface switched to the *cis* isomer, corresponding to an increase of the switching capability of more than 100% with respect to the original **7-SAM**. The performance of the self-diluting SAM was thus superior to results for alkyl-based glyco-SAMs, the maximum switching capacity of which (using a diluent compound) was determined as 4%.[6] From Figure 5b, d, it is also clear that the *cis*/*trans* isomerization was fully reversible. By alternating irradiation with light of 440 nm and 365 nm, it was possible to switch the glyco-SAM back and forth with a constant intensity change of $\Delta I_{exp} = 5\%$ (see the Supporting Information, Figure S17). Interestingly, if compound **7** was deprotected in solution and subsequently deposited on the surface, the resulting **8-SAM** (deprotection in solution before surface deposition) showed only very weak changes ($\Delta I_{exp} < 1\%$) in the intensity of the C_{aryl}–O vibration after irradiation with light of 365 nm (see the Supporting Information, Figure S20). This indicates that the improvement of the switching behavior was only observed when the TBDPS protecting group was cleaved on the surface, and underlines the feasibility of the self-dilution concept towards photoswitchable SAMs.

Surface spectroscopic investigation of rigid glyco-SAMs

For the fabrication of rigid glyco-SAMs, the azobenzene mannosides **14**, **20**, and **21** were employed. They were deposited on Au(111) from solutions in methanol/acetone (95:5), and the resulting monolayers were investigated by means of XPS, NEXAFS, and IRRAS.

X-ray photoelectron spectroscopy

The XPS data of **20-SAM** are shown in Figure 6. The C 1s spectrum (Figure 6a) comprises three different signals. The main component at 284.6 eV (59%, red) can be assigned to aromatic carbon atoms bound to each other or to sulfur. A smaller signal at 285.5 eV (7%, blue) corresponds to the carbon atoms bound to nitrogen. The third species (29%, green) at 286.5 eV can be ascribed to carbon atoms bound to oxygen. The anomeric carbon atom, which is bound to two oxygen atoms, contributes to a fourth signal at 288.0 eV (5%, orange). Again, the relative fractions of the different species fit well to the chemical composition (62:8:25:5) of compound **20**. The S 2p spectrum (Figure 6b) features only one doublet at 162.0 and 163.3 eV (100%, red), corresponding to a thiolate species.[28–30] Importantly, no disulfide or other sulfur-containing impurities are detectable. This clearly reflects the high purity of the SAM and furthermore proves the covalent attachment of the molecule to the surface. The N 1s spectrum also shows only one component (100%, blue) at 399.6 eV, which corresponds to the azo moiety of the **20-SAM** (Figure 6c).[6,26,27] In conclusion, the XP spectra confirm the presence of a monolayer of compound **20** (**20-SAM**) in high purity.

Near-edge X-ray absorption fine structure spectroscopy

NEXAFS spectra were measured at the carbon and nitrogen K-edges for monolayers of azobenzene mannoside **20** on Au(111) single crystals. The carbon K-edge spectrum, shown in Figure 6d, exhibits a prominent resonance at 285.4 eV, which can be assigned to a 1s→π^* (LUMO) transition. This resonance displays a decreasing intensity from 90° to 30°. The second π^* resonance is located at 287.4 eV and the third at 298.7 eV, and these features show almost no angular dependence. At higher energy (293.8 eV), several broadened σ^* resonances can be observed.

The nitrogen K-edge NEXAFS in Figure 6e reveals one prominent resonance at 399.0 eV. The energy of this feature again corresponds to the N 1s-to-π^* transition reported in the literature for azobenzene units.[27] The difference spectrum (red) shows that this transition exhibits a marked angular dependence. The tilt angle β of compound **20** with respect to the surface normal amounts to $23 \pm 6^\circ$ (see the Supporting Information, Figure S12), in good agreement with results for other bi-

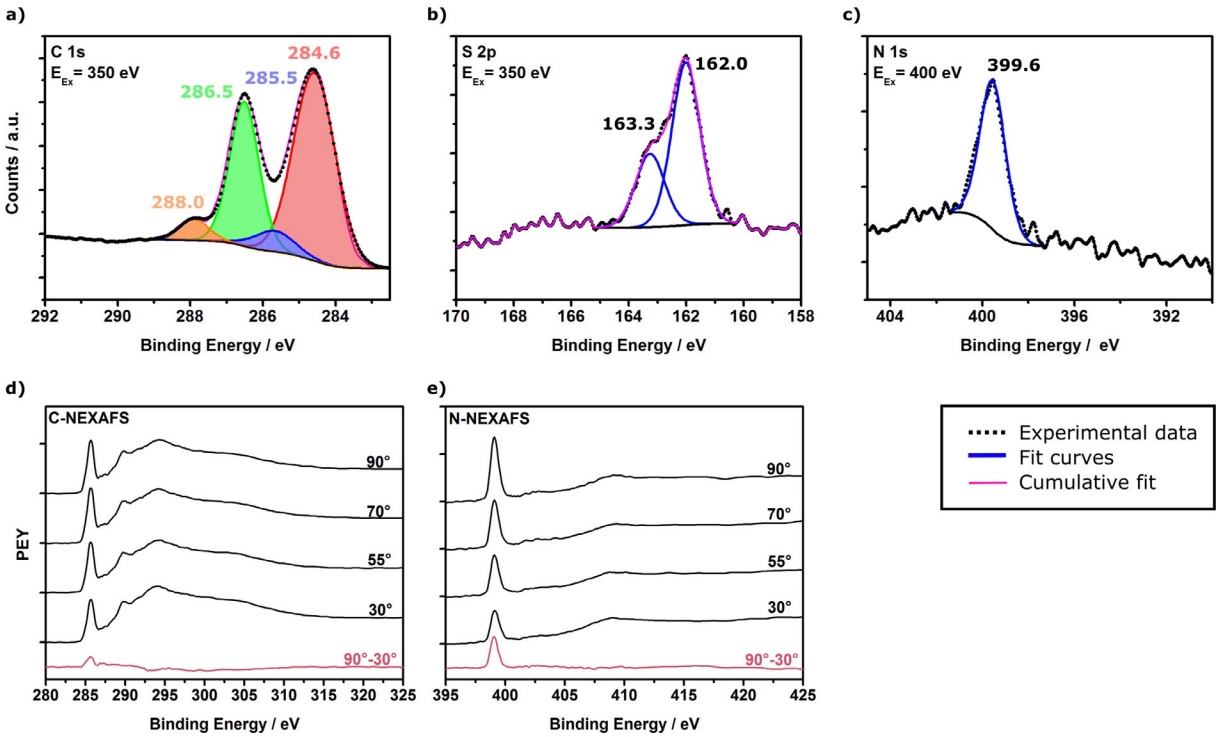

Figure 6. XP spectra and normalized NEXAFS spectra at different angles of **20-SAM** adsorbed on Au(111). The a) C 1s, b) S 2p, and c) N 1s regions are shown. The baseline is shown in black, the measured data are represented by black dots, and the fitted sum spectrum is illustrated by the magenta line. d) C *K*-edge, and e) N *K*-edge spectra are shown. The difference spectra (90°–30°) are shown in red.

phenyl-based SAMs reported in the literature.[34] These results are in accordance with the carbon K-edge NEXAFS data.

Infrared reflection absorption spectroscopy

Besides XPS and NEXAFS, IRRAS was also employed to investigate compound **20** adsorbed as a monolayer on Au(111), in particular its switching properties. Intensities of around 10^{-3} absorbance units again reflect the formation of a monolayer on Au(111) (Figure 7 a).[14] The measured bulk IR and IRRA spectra closely resemble the calculated bulk IR spectrum. By reference to the calculated spectrum, the bands appearing in the measured spectra can be assigned to specific vibrational modes. The vibrational mode at 1600 cm^{-1} in the IRRA spec-

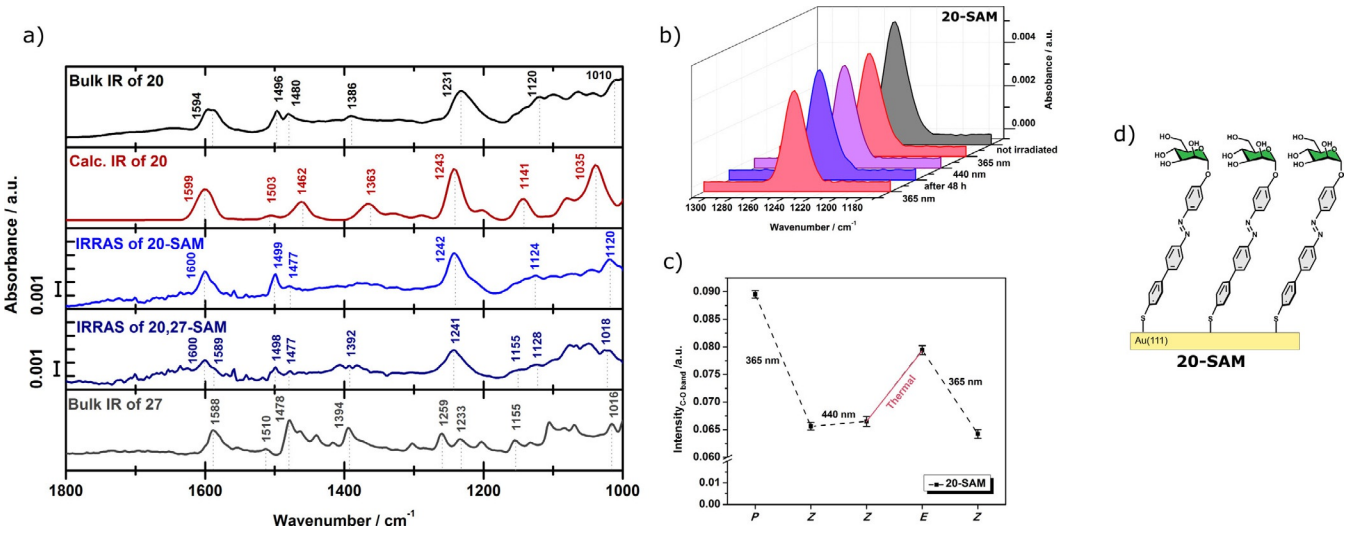

Figure 7. a) Schematic illustration of compound **20** in a monolayer on Au(111); b) measured bulk IR spectra of **20** (black) and **27** (grey) and IRRA spectra of the **20-SAM** (light-blue) and the **20,27-SAM** (dark-blue) in comparison with the computed bulk IR spectrum (red) of compound **20**. c) PM-IRRA spectra in the C_{aryl}–O region of the **20-SAM** before (grey) and after irradiation with light of 365 nm (red), followed by irradiation at 440 nm (purple); spectrum after thermal relaxation (blue); d) intensity of the C_{aryl}–O stretching vibration after irradiation with light of 365 nm, followed by irradiation at 440 nm and thermal relaxation for the **20-SAM**.

trum corresponds to C_{aryl}–C_{aryl} stretching vibrations of the biphenyl unit. In the IRRA spectrum, the bands at 1499 and 1477 cm^{-1} exhibit a different intensity ratio to that in the bulk IR spectrum due to the surface selection rule.[32] These bands can be assigned to N=N stretching and aromatic C–C stretching vibrations, respectively.

A very prominent C_{aryl}–O stretching vibration can be observed at 1242 cm^{-1} in the surface IR spectrum and at 1231 cm^{-1} in the bulk IR spectrum (Figure 7b). In analogy to the situation for **7-SAM** described above, this vibration is well suited for monitoring the *cis*/*trans* isomerization of **20-SAM** by PM-IRRAS.[6] The first measurement (gray in Figure 7c) shows the spectrum of the unirradiated sample. After irradiation with light of 365 nm, the intensity of the C_{aryl}–O vibration decreased by $\Delta I_{exp} = 27\%$ (red) (Figure 7d). This reflects the *trans*→*cis* isomerization of the **20-SAM** and the corresponding orientational change of the transition dipole moment of the C_{aryl}–O stretch. The possible orientations of the C_{aryl}–O stretch in the *cis* isomer were determined in analogy to those in the azobenzene mannosides **7** and **8** with a flexible backbone (see above). Based on the rotationally averaged *cis* configuration C, a decrease of $\Delta I_{theo} = 80\%$ of the C_{aryl}–O intensity is predicted. From the observed intensity decrease, it can be concluded that more than one-third of the molecules (34%) in the **20-SAM** switch to the *cis* isomer (Table 1). Remarkably, therefore, the switching capacity of **20-SAM** exceeds those obtained for SAMs formed from compounds **7** and **8** by almost one order of magnitude.

With a view to switching *cis*-**20-SAM** back to the *trans* isomer, the sample was irradiated with light of wavelength 440 nm. Surprisingly, however, no increase in the C_{aryl}–O stretching intensity was observed (Figure 7c, d). Thus, it was concluded that it is not possible to photochemically switch the SAM back to the *trans* configuration. However, after leaving the sample for 48 h at room temperature under N_2 atmosphere, a slight increase (+8% intensity) of the C_{aryl}–O band could be observed, which we attribute to a thermal relaxation process. This small amount of *trans* isomer could, in turn, be switched back to the *cis* state by irradiation with light of 365 nm.

The described results indicate a high thermal stability of ***cis*-20-SAM** on Au(111). Since similar SAMs devoid of a sugar head group show reversible *cis*/*trans* isomerization,[16] we assume intermolecular interactions within the SAM to be responsible for the observed behavior. Hydrogen bonds of the D-mannose head group of the SAM could stabilize the *cis* isomer on the surface and prevent *cis*→*trans* back isomerization. In order to probe such an effect of the free hydroxy groups of the sugar ring, the *O*-allylated analogue of **20**, mannoside **21** was employed and deposited on an Au(111) surface from a 1 mM solution in methanol/acetone (95:5). The obtained film was investigated by XPS, NEXAFS, and IRRAS (see the Supporting Information, Figures S4, S10, and S19), which again revealed a highly pure and well-oriented monolayer of **21** on Au(111). The tilt angle β of the molecules within the **21-SAM** was determined as $24 \pm 5^\circ$ ($\Delta I_{theo} = 78\%$ based on the orientationally averaged *cis* configuration C), quite similar to that of the parent **20-SAM**. The switching properties of the **21-SAM** were elucidated by PM-IRRAS, and the resulting spectra are shown in Figure 8a–c. Upon irradiation of the sample with light of 365 nm, the intensity of the C_{aryl}–O stretching vibration decreased by $\Delta I_{exp} = 9\%$. Again, this intensity change can be attributed to the *trans*/*cis* isomerization of compound **21** adsorbed on the surface. After irradiation with light of 440 nm, the intensity increased once more. The switching capacity calculated on the basis of ΔI_{exp} and ΔI_{theo} amounted to 12%. Consequently, this process is reversible for **21-SAM** (Figure 8a–c), in contrast to the situation for the parent **20-SAM**. However, the intensity change is noticeably lower than that for the original **20-SAM**.

From the described results, we conclude that the free OH groups of the mannoside head groups of **20-SAM** stabilize the *cis* isomer on the surface through intermolecular hydrogen bonds, preventing the molecules from reverting to the *trans* state upon irradiation with light of 440 nm. Otherwise, when the hydroxy groups are protected, stabilization of the *cis* isomer by H-bonds is no longer possible and the switching process becomes reversible. On the other hand, the steric demand of the head group is drastically increased by four allyl protecting groups, which lowers the free volume within the SAM. For this reason, the switching capacity of **21-SAM** is distinctly lowered in comparison to that of **20-SAM**.

In addition to the rigid *p*-mannosyloxy-*p'*-phenyl-azobenzene derivative **20** and its protected analogue **21**, the isomeric glycoazobenzene derivative **14** was tested, in which the azobenzene moiety is shifted one phenyl group further away from the sugar ring, leading to a *p*-mannosyloxyphenyl-azobenzene structural motif (see Scheme 2). A monolayer of this molecule was deposited on gold and investigated by XPS, NEXAFS, and IRRAS as before (see the Supporting Information, Figures S5, S11, and S21). The tilt angle of **14-SAM** with respect to the surface normal was determined as $\beta = 29 \pm 3^\circ$ ($\Delta I_{theo} = 73\%$, based on configuration C). Upon irradiation with light of 365 nm and 440 nm, a reversible change of $\Delta I_{exp} = 5\%$ could be observed for the C_{aryl}–O stretching vibration intensity, corresponding to a switching capacity of 7% for **14-SAM**. This much lower value compared to those of **20-SAM** (34%) and **21-SAM** (12%) can be rationalized in terms of the large free volume required for reorientation of the mannosyloxybiphenyl moiety "above" the azo group as compared to the shorter mannosylphenyl portion that terminates **20-SAM**. This result demonstrates that the biphenyl group should be placed *below* (and not *above*) the azo function to obtain satisfactory switching behavior of the respective glyco-SAM on an Au(111) surface.

Investigation of mixed rigid SAMs

In order to increase the lateral distance between the head groups and reduce their intermolecular interactions, **20-SAM** was diluted with the azobenzene derivative **27** lacking the mannose unit. Mixed SAMs were fabricated by immersing the substrate in a solution containing both compounds, with the diluent molecule **27** and **20** in a ratio of 4:1, which was found to be optimal in our earlier studies with diluted SAMs.[6] More-

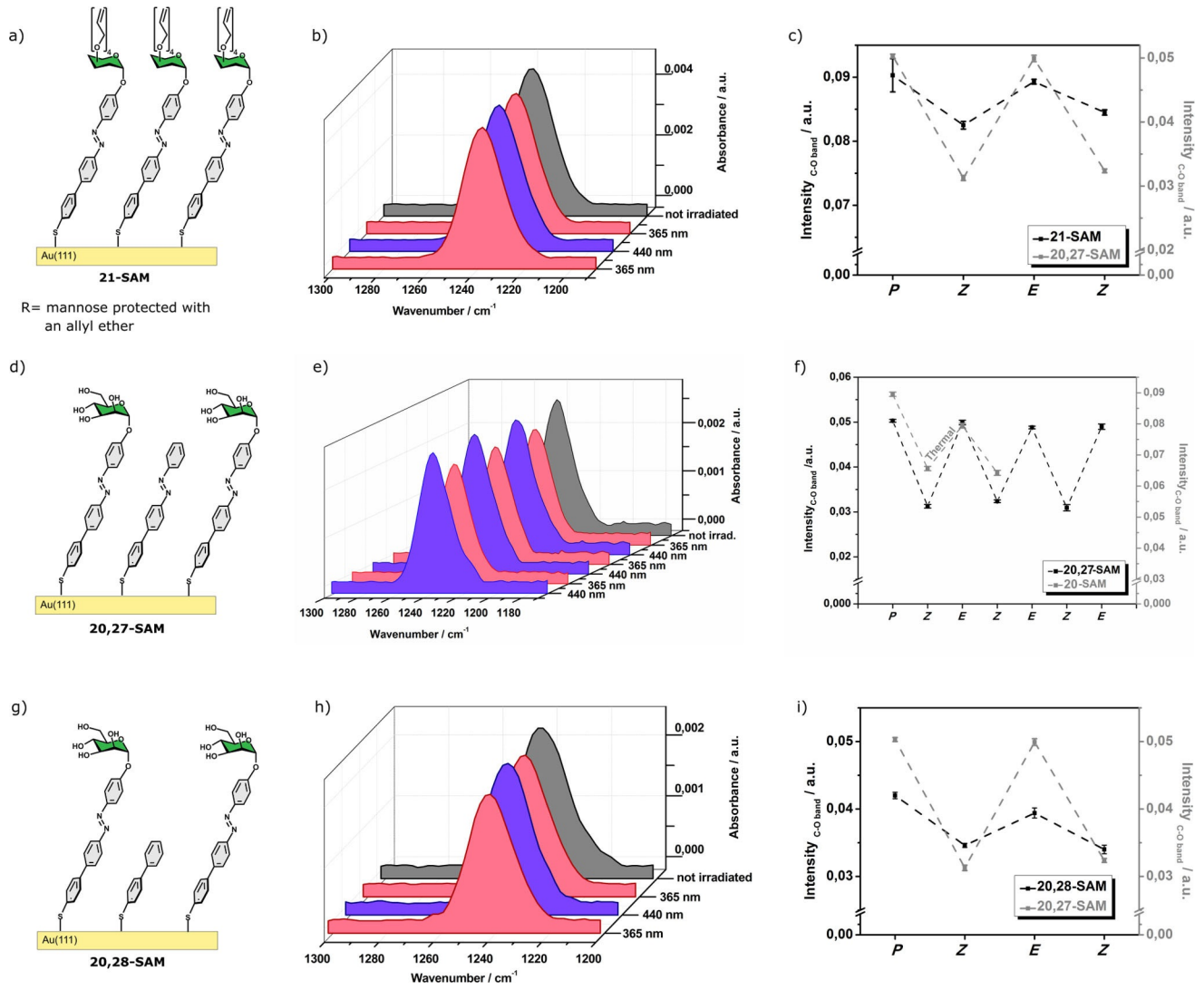

Figure 8. a) Schematic illustration of the **21-SAM**. b) PM-IRRA spectra of the C_{aryl}–O region of the **21-SAM** before and after irradiation with light of 365 nm and 440 nm. c) Changes in the intensity of the C_{aryl}–O stretching vibration after irradiation with light of 365 nm or 440 nm for the **21-SAM** (black) in comparison with data for the **20,27-SAM** (grey). d) Schematic illustration of the **20,27-SAM**. e) PM-IRRA spectra of the C_{aryl}–O region of the **20,27-SAM** before and after irradiation with light of 365 nm and 440 nm. f) Changes in the intensity of the C_{aryl}–O stretching vibration after irradiation with light of 365 nm or 440 nm for the **20,27-SAM** (black) in comparison with data for the pure **20-SAM** (grey). g) Schematic illustration of the **20,28-SAM**. h) PM-IRRA spectra of the C_{aryl}–O region of the **20,28-SAM** before and after irradiation with light of 365 nm and 440 nm. i) Changes in the intensity of the C_{aryl}–O stretching vibration after irradiation with light of 365 nm or 440 nm for the **20,28-SAM** (black) in comparison with data for the **20,27-SAM** (grey).

over, it is known that the ratio of components assembled in an SAM is not necessarily the same as that in the solution used for immersion of the gold wafer.[10]

To check the purity, composition, and orientation of the mixed **20,27-SAM**, XPS and NEXAFS measurements were conducted (see the Supporting Information, Figures S2 and S8). The composition in the C 1s XP spectrum reflects a 1:1 ratio of compounds **20** and **27** in the surface-adsorbed SAM. This is consistent with the observation that the intensity of the C_{aryl}–O stretching vibration in the surface IR spectrum is reduced by about 50% (Figure 7a). The NEXAFS data for the **20,27-SAM** and the pure **20-SAM** are almost identical, because the most intense NEXAFS resonances originate from the benzene and azo units of the molecules. This suggests that the dilution of the SAM does not influence the orientation of the molecules. The tilt angle β of the **20,27-SAM** with respect to the surface normal determined by NEXAFS was $22 \pm 4^{\circ}$ ($\Delta I_{theo} = 80\%$, based on orientation C). The IRRA spectrum of the mixed **20,27-SAM** in Figure 7a still shows the same vibrations as seen for pure **20-SAM**. This is reasonable, because the structure of diluent molecule **27** is very similar to that of its glycosylated analogue **20**. The C_{aryl}–O stretching vibration is still very prominent, but less intense than that for pure **20-SAM**. In addition, a shoulder can be seen at 1215 cm^{-1}, which can be assigned to a C–N stretching vibration combined with a C_{aryl}–C_{aryl} stretching vibration of the azobenzene moiety in the diluent molecules.

In order to investigate the switching behavior of the mixed **20,27-SAM**, PM-IRRAS was employed in the spectral region of the C_{aryl}–O stretch. After irradiation with light of 365 nm, the

intensity of the C_{aryl}–O stretching mode decreased in the surface IR spectrum by $\Delta I_{exp} = 38\%$ due to the *trans*/*cis* isomerization and the associated change in orientation with respect to the surface (see the Supporting Information, Figure S15). This corresponds to a switching capacity of 48%, even larger than that observed for pure **20-SAM**. That is to say, nearly half of the molecules (48%) in **20**,**27-SAM** were switched from the *trans* to the *cis* state. Moreover, as shown in Figure 8d–f, this process was fully reversible. Thus, by dilution of **20-SAM** with compound **27**, a reversible *cis*/*trans* isomerization of this glyco-SAM is enabled.

In a final step, a different diluent compound to that in **20**,**27-SAM** was employed, in order to probe the influence of the incorporated azobenzene unit (as in **27**) on the switching properties of a mixed glyco-SAM. To this end, 4-biphenylthiol (**28**, see Scheme 4) was employed as a non-photoswitchable diluent molecule, and **20**,**28-SAM** on Au(111) was prepared. The sample was deposited from a 1 mM solution of compounds **20** and **28** (1:4) in a methanol/acetone mixture (95:5). XPS, NEXAFS, and IRRAS data again proved that the SAM was of high purity and that the composition of **20**,**28-SAM** was 1:1 (see the Supporting Information, Figures S3 and S9). The orientation of **20**,**28-SAM** was determined by NEXAFS. At $24 \pm 3^\circ$ ($\Delta I_{theo} = 78\%$, based on orientation C), the tilt angle is again very similar to that of **20-SAM** (see the Supporting Information, Figure S12). Figure 8g–i shows PM-IRRAS data for the **20**,**28-SAM**. Upon irradiation of the sample with light of 365 nm, the intensity of the C_{aryl}–O stretching vibration decreased by $\Delta I_{exp} = 18\%$. Although this process proved to be reversible, the switching behavior was significantly inferior to those than for pure **20-SAM** and mixed **20**,**27-SAM**. Thus, we conclude that the azobenzene moiety is an essential part of the diluent molecule for obtaining efficient and reversible switching properties of the respective glyco-SAM.

Lectin binding tests

For a first biological evaluation of the effect of *trans*/*cis* isomerization of the new glyco-SAMs on carbohydrate recognition, the fluorescein-labeled lectin Concanavalin A (ConA-FITC) was used. This well-known lectin shows a strong specificity for α-D-mannosyl residues, making it suitable for binding studies with our SAMs. Three different monolayers were selected for the tests, pure **20-SAM**, with a switching capacity of 34% (see Table 1), its diluted version **20**,**27-SAM**, which performed best among all of the investigated SAMs with a switching capacity of 48%, as well as **8-SAM**, which showed almost no *cis*/*trans* isomerization on the surface. The respective SAMs were subdivided into two halves and irradiated with light of 365 nm (to effect *trans*→*cis* isomerization) or 485 nm (to effect *cis*→*trans* isomerization). The wafers were then incubated with ConA-FITC and, after washing, fluorescence of the bound lectin was recorded (see the Supporting Information, Figure S84). Strikingly, lectin binding to **20-SAM** was reduced by 28% after irradiation with light of 365 nm, whereas **20**,**27-SAM** after the same *trans*→*cis* isomerization step showed 33% reduced lectin binding compared to its *trans* state. These data parallel the determined switching capacities of the SAMs (34% and 48%), but also show that additional effects besides *trans*→*cis* isomerization add to carbohydrate recognition on the surface. This finding is not unexpected and might be interpreted in terms of the tetrameric nature of ConA at pH > 6. In line with the spectroscopic investigation, irradiation of **8-SAM** had no significant effect on lectin binding. In future experiments, *cis*/*trans* isomerization of the hitherto available glyco-SAMs will be investigated in different biological systems to advance our understanding of the biological effect of carbohydrate ligand orientation on surfaces.

Conclusions

The switching capacity of glyco-SAMs is of fundamental importance for their biological function. Therefore, it has been our goal to design glycoazobenzene thiols for the fabrication of glyco-SAMs on Au(111) with high switching capacity. To this end, it was important to form stable SAMs and concomitantly provide enough free volume for the reversible *cis*/*trans* photoisomerization. We have varied key molecular parameters, in particular protecting groups on the sugar ring and backbone rigidity of the immobilized molecules, to investigate their influence on the physicochemical properties of the respective glyco-SAMs, most notably their switching behavior.

Six new azobenzene mannosides have been synthesized and characterized as bulk materials and in solution, whereby all of them showed reversible *cis*/*trans* isomerization. They were then deposited on an Au(111) surface, and the composition and packing density of the formed SAMs were spectroscopically characterized through a combination of IRRAS and NEXAFS. XPS data were used to determine the chemical compositions of the SAMs and proved their high purities. It was also possible to verify the deprotection "on SAM" by inspection of the Si 2p region of the XP spectrum. The molecular orientation of the SAMs with respect to the surface was determined by NEXAFS spectroscopy. For the alkyl SAMs, a tilt angle β with respect to the surface normal of 32–33° was obtained; for the rigid SAMs, the tilt angle β was found to be in the range 22–24°. Both results are consistent with previous studies reported in the literature.

The switching behavior of the glyco-SAMs was investigated with the aid of IRRAS. Based on the intensity change of the C_{aryl}–O stretching vibration upon *cis*/*trans* isomerization and the orientation of the molecules determined by NEXAFS, the switching capacities of the different glyco-SAMs were assessed. The approach of self-dilution within the glyco-SAM leads to an improvement of the inherently low switching capacities by more than 100% (**7-SAM**: 3%; **7-SAM^{deprot}**: 7%). Much higher switching capacities could be obtained by using SAMs with rigid spacers. In pure **20-SAM**, 34% of the molecules switched from *trans* to the *cis* isomer upon irradiation with light of 365 nm. However, **20-SAM** could not be switched back to *trans* state by irradiation with light of 440 nm. Instead, only a slow thermal relaxation could be observed. By protecting the OH groups of the mannose moiety, the reversibility of the *cis*/*trans* isomerization was restored (**21-SAM**), albeit with loss of

switching capacity. In contrast, diluting the rigid SAMs was found to both improve the switching capacity and enable reversible switching. In **20**,**27-SAM**, almost half of the molecules underwent reversible *trans*/*cis* isomerization (48%). These switching properties are unprecedented and mark significant progress in the field of photoswitchable glyco-SAMs. It was found to be necessary that the diluent compound also contains an azobenzene moiety, at the same position as in the glyco compound. Otherwise, the switching capacity decreases sharply (**20**,**28-SAM**; 23%). First lectin assays with ConA showed that the observed differences in lectin binding mirror the switching capacities of the SAMs, but that the determined lectin binding differences are smaller than the *cis*/*trans* ratios of the investigated SAMs.

In conclusion, this study provides new and detailed information about different approaches towards photoswitchable glyco-SAMs. Eventually, these surfaces will be employed to further improve the photoswitchability of cell adhesion compared to already established systems[6,7] and to advance our understanding of the underlying effects.

Experimental Section

General procedures

Chemicals were purchased from Sigma–Aldrich, Acros Organics, or TCI and were used without further purification. Moisture-sensitive reactions were carried out in dry glassware under a positive pressure of nitrogen. Before adding tetrakis(triphenylphosphine)palladium(0), the reaction mixtures were degassed by three freeze–pump–thaw (F-P-T) cycles. Otherwise, flasks containing the reaction mixtures were sonicated in an ultrasonic bath for 10 min. Thin-layer chromatography was performed on silica gel plates (GF, 254, Merck). Spots were visualized under UV light and/or by spraying with vanillin/10% sulfuric acid in ethanol followed by heat treatment. Flash chromatography was performed on silica gel 60 (Merck, 230–400 mesh, particle size 0.040–0.063 nm) using distilled solvents. Optical rotations were measured with a Perkin-Elmer 241 polarimeter (sodium D-line: 589 nm, length of cell: 1 dm) in the noted solvents. ^{1}H, ^{13}C, and ^{11}B NMR spectra were recorded with Bruker DRX-500 and AV-600 spectrometers. Chemical shifts are reported relative to internal tetramethylsilane or the residual proton signal of the deuterated solvent. All NMR spectra of the *E*-isomers of the azobenzene derivatives were recorded after samples were kept for 16 h in the dark at 40 °C. IR spectra were measured on a Perkin-Elmer FTIR Paragon 1000 (ATR) or a Perkin-Elmer Lambda 650 spectrometer, and are reported in cm^{-1}. Elemental analyses were performed with a Euro EA 3000 from Euro Vektor and a Vario Micro cube from Elementar. Thermal *cis*/*trans* isomerization was assessed by recording ^{1}H NMR spectra on a Bruker ARX 300 spectrometer.

Gold substrates

Glass substrates with a 50 Å titanium adlayer and a 200 nm vapor-deposited gold film from EMF Corporation (Ithaca, NY) were used for IRRAS measurements. XPS and NEXAFS measurements were made with sputtered Au(111) single crystals.

Preparation of monolayers

Monolayers of **7** and **8** were prepared by immersing Au(111) substrates in 0.5 mM solutions of the respective compounds in methanol at room temperature. Monolayers of **14**, **20**, **21**, **27**, and **28**, as well as the respective mixed SAMs, were prepared by immersing Au(111) substrates in 0.5 mM solutions of the respective compounds in methanol/acetone (95:5) at room temperature. After immersion for 48 h, the sample was removed from the solution, rinsed with methanol and acetone, and dried in a stream of nitrogen.

IRRAS

The surface-adsorbed molecules were investigated by means of a Bruker Vertex 70 FTIR spectrometer equipped with a polarization modulation accessory (PMA) 50 unit (Bruker Optik GmbH, Ettlingen, Germany). This instrument allows the acquisition of IRRAS and PM-IRRAS data over the spectral range from 4000 to 800 cm^{-1}. IRRAS data were collected with a liquid-nitrogen-cooled MCT detector in a horizontal reflection unit for grazing incidence (Bruker A518). The sample chamber was purged with dry nitrogen before and during measurements. A deuterated hexadecane-thiol SAM on Au(111) was used as a reference for the background spectrum for conventional IRRA spectra. Each spectrum was accumulated from 2048 averaged spectra. A p-polarized beam at an incident angle of 80° to the surface normal was used for measurements. All spectra were recorded with 4 cm^{-1} resolution. PM-IRRAS data for the switching experiments were collected with the PMA 50 accessory using a liquid-nitrogen-cooled MCT detector. The PEM maximum efficiency was set for the half-wave at 1750 cm^{-1} for analysis of the area from 1400 to 1100 cm^{-1}. All spectra were recorded with 4 cm^{-1} resolution.

IRRAS and PM-IRRAS data were processed using OPUS software Version 6.5 (Bruker, Germany). Baseline correction of the resulting IRRAS data was performed by the rubber band method in an interactive mode. PM-IRRAS data were processed by implicit removal of the Bessel function through manual baseline correction. For the *trans*/*cis* isomerization of different compounds adsorbed on Au(111), the prepared samples were irradiated within the spectrometer using an LED [Nichia NC4U133(T), peak wavelength: 365(±9) nm or 440(±5) nm, 1 LED, power dissipation: 12 W, luminous flux: 10 lm, distance≈5 cm]. The sample was irradiated at the selected wavelength for 10 min.

Due to the small shoulder in the investigated IR band (C_{aryl}–O stretching vibration) at lower wavenumbers, the band was fitted with two Gaussians to determine the intensity of the C_{aryl}–O band (see the Supporting Information, Figures S14–S19). The second band corresponds to a C–H bending vibration within the mannose moiety. As this vibration is a combination of different vibrations, and the mannose moiety can rotate about the C_{aryl}–O bond, the orientation of this vibration is barely affected by the isomerization process and could thus be neglected.

In order to calculate the expected intensity change ΔI_{theo}, different orientations of the *cis* isomer have to be taken into account, as the molecules within the SAM can rotate about their axes. The orientations A (head group downwards) and B (head group upwards) were calculated on the basis of the tilt angle β, which was obtained from NEXAFS data. Using Equations (1) and (2), the expected intensity change of the C_{aryl}–O stretch in the surface IR spectrum could be calculated:

$$\Delta I_{theo} = I_{trans}(1 - R_{theo}) \quad (1)$$

$$R_{theo} = \frac{cos^2\varphi_{cis}}{cos^2\beta} \quad (2)$$

Since a distribution of orientations of the head group, rather than one specific orientation, can be assumed within the glyco-SAM, another orientation was introduced, denoted as C. Orientation C describes an averaging over all possible angles of the transition dipole moment of the C_{aryl}—O stretch. The averaged intensity of the *cis* isomer was calculated according to Equation (3):[35]

$$\overline{I_{cis}} = \frac{1}{3}\left[\frac{1}{2}(3cos^2\beta - 1)(3cos^2(180-\gamma) - 1) + 1\right] \quad (3)$$

where the angle γ is that between the molecular axis and the transition dipole moment of the C_{aryl}—O stretch in the *cis* isomer.

XPS and NEXAFS

XPS and NEXAFS measurements were performed at the BESSY II synchrotron radiation facility using the PREVAC endstation at the beamline HE-SGM. The experimental station is equipped with a hemispherical VG Scienta R3000 photoelectron analyzer. The energy resolution E/DE of the beamline with 150 mm slits is 800. XP survey spectra were acquired at 700 eV photon energy using an analyzer pass energy of 100 eV, whereas for the C 1s, Si 2p, and S 2p spectra the photon energy used was 350 eV with a pass energy of 50 eV. For N 1s spectra, the photon energy was 500 eV with a pass energy of 50 eV.

All spectra were acquired at normal electron emission. For determination of the relative composition of the adlayers, the XP spectra were energy-corrected using the Au $4f_{7/2}$ line at a binding energy of 84.0 eV as a reference. Background correction was performed using a combination of a Shirley and a linear background for all signals. Peak fitting was performed using the program CASA XPS. The maximum deviation of full-width at half-maximum of the fitted Gaussian within a spectrum was set at 0.2 eV. The fitting parameters are shown in Tables S1–S7 in the Supporting Information. All spectra were smoothed by the SG quadratic method (CASA XPS, smoothing width = 5) in order to improve the signal-to-noise ratio. Care was taken to ensure that this process did not alter the form of the spectrum.

To correct for the photon flux of the NEXAFS measurements, all spectra were modified by subtracting the spectrum obtained for a freshly sputtered clean gold substrate and then edge-step-normalized (using the average intensities for the C K-edge between 275 ± 0.5 eV and 320 ± 0.5 eV and for the N K-edge between 395 ± 0.5 eV and 420 ± 0.5 eV as pre- and post-edge). The normalized spectra were fitted by employing a step function for the absorption edge and Gaussians for the π* and σ* resonances in order to determine the intensities I of specific resonances. In all spectra, the width of the step function was set at 0.2 eV. The series of spectra of a specific sample measured at different angles of incidence were fitted with the same parameter set; that is, the energies of the resonances were allowed to vary at most by 0.2 eV and the half-widths at full-maximum by 0.3 eV, in agreement with the estimated experimental resolution. To determine the orientation of the molecular orbitals, the angular dependences of the intensities I of the π* resonances were finally fitted to model functions for the angular dependence (see the Supporting Information, Figure S12) according to Equation (4):[36]

$$I = A\left[Pcos^2\theta\left(1 - \frac{3}{2}sin^2\beta\right) + \frac{1}{2}sin^2\beta\right] \quad (4)$$

where A are the specific amplitudes of the resonances, P is the degree of polarization (0.91), θ is the angle of incidence, and β is the tilt angle of the transition dipole moment of the molecule with respect to the surface normal. The specified errors for the tilt angles were derived from the fit.

Synthesis and analytical data of target molecules 6, 7, 13, 14, and 18–21 (Figure 9; for all data, see the Supporting Information)

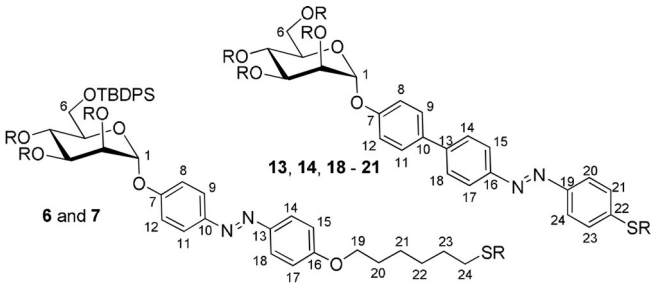

Figure 9. Compound numbering as used for the assignment of NMR spectroscopic data.

(*E*)-*p*-{*p*′-[6-(Acetylthio)hexoxy]phenylazo}phenyl 2,3,4-tri-*O*-acetyl-6-*O*-*tert*-butyldiphenylsilyl-α-D-mannopyranoside (6): The mannosyl donor **4** (337 mg, 905 μmol) and the azobenzene derivative **5** (124 mg, 333 μmol) were dissolved in dry dichloromethane (4 mL). The solution was cooled to 0 °C, whereupon BF_3 etherate (0.17 mL, 1.36 mmol) was added. The reaction mixture was allowed to warm to room temperature and stirred for 2 h. It was then quenched by the addition of saturated aqueous $NaHCO_3$ solution (4 mL), the phases were separated, and the organic phase was dried over $MgSO_4$, filtered, and concentrated under reduced pressure. Column chromatography (toluene/ethyl acetate, 9:1) gave the product as an orange solid (258 mg, 287 μmol, 86%). R_f = 0.40 (toluene/ethyl acetate, 9:1); m.p. 139 °C; $[\alpha]_D^{20} = +108.5$ (c = 0.73, ethyl acetate); ^{1}H NMR (500 MHz, $CDCl_3$): δ = 7.89–7.81 (m, 4H; H-9, H-11, H-14, H-18), 7.67–7.62 (m, 4H; TBDPS-aryl-H_{ortho}), 7.44–7.34 (m, 6H; TBDPS-aryl-H_{meta}, -H_{para}), 7.20–7.17 (m, 2H; H-15, H-17), 7.00–6.97 (m, 2H; H-8, H-12), 5.60 (d, $^3J_{1,2}$ = 1.8 Hz, 1H; H-1), 5.56 (m, 2H; H-3, H-4), 5.45 (dd, $^3J_{1,2}$ = 1.9 Hz, $^3J_{2,3}$ = 3.2 Hz, 1H; H-2), 4.03 (t, J = 6.5 Hz, 2H; H-19), 3.92 (ddd, $^3J_{4,5}$ = 9.3 Hz, $^3J_{5,6a}$ = 4.5 Hz, $^3J_{5,6b}$ = 1.9 Hz, 1H; H-5), 3.76 (dd, $^3J_{5,6a}$ = 4.6 Hz, $^2J_{6a,6b}$ = 11.6 Hz, 2H; H-6a), 3.67 (dd, $^3J_{5,6b}$ = 2.0 Hz, $^2J_{6a,6b}$ = 11.6 Hz, 2H; H-6b), 2.90 (t, J = 7.3 Hz, 2H; H-24), 2.33 (s, 3H; SCOCH_3), 2.18, 2.05, 1.92 (each s, each 3H; 3 OAc), 1.85–1.79 (m, 2H; H-20), 1.65–1.59 (dt, J = 14.7 Hz, J = 7.4 Hz, 2H; H-23), 1.53–1.42 (m, 4H; H-21, H-22), 1.03 ppm (s, 9H; C(CH_3)$_3$); ^{13}C NMR (126 MHz, $CDCl_3$): δ = 196.6 (SCOCH$_3$), 170.2, 170.1, 169.5 (3 COCH$_3$), 161.4 (C-16), 157.5 (C-7), 148.3 (C-13), 146.9 (C-10), 135.8 (TBDPS-aryl-C_{ortho}), 135.6 (TBDPS-aryl-C_{ortho}), 133.3 (TBDPS-aryl-C_{ipso}), 133.0 (TBDPS-aryl-C_{ipso}), 129.7 (TBDPS-aryl-C_{para}), 129.7 (TBDPS-aryl-C_{para}), 127.7 (TBDPS-aryl-C_{meta}), 127.6 (TBDPS-aryl-C_{meta}), 124.5 (C-14, C-18), 124.2 (C-9, C-11), 116.7 (C-15, C-17), 114.7 (C-8, C-12), 95.7 (C-1), 72.0 (C-5), 69.6 (C-2), 69.2 (C-3), 68.1 (C-19), 65.9 (C-4), 62.3 (C-6), 30.7 (SCOCH_3), 29.4 (C-23), 29.0 (C-19), 29.0 (C-20), 28.5 (C-22), 26.6 (C(CH_3)$_3$), 25.6 (C-21), 20.8, 20.8, 20.6 (3 COCH_3), 19.2 ppm (C(CH$_3$)$_3$); IR (ATR): $\tilde{\nu}$ = 2932, 2857, 1752, 1213, 1106, 702, 502 cm^{-1}; MS (ESI): m/z: calcd for $C_{48}H_{58}N_2O_{11}SSi$: 899.3603 [M]; found: 899.3589.

(*E*)-*p*-{*p*′-[6-(Thio)hexoxy]phenylazo}phenyl-6-*O*-*tert*-butyldiphenylsilyl-α-D-mannopyranoside (7): The protected mannoside **6** (250 mg, 278 μmol) was dissolved in dry methanol (2 mL), and sodium methanolate solution (20 μL, 5.4 M in methanol) was added. After stirring for 3 h at room temperature, the solution was neutralized with Amberlite IR120 ion-exchange resin. The resin was filtered off and the filtrate was concentrated under reduced pressure. After filtration through silica, the product was obtained as an orange solid (200 mg, 273 μmol, 90%). $[\alpha]_D^{20} = +20.0$ ($c = 0.6$, CH_2Cl_2); ^{1}H NMR (500 MHz, $CDCl_3$): $\delta = 7.87–7.84$ (m, 2H; H-14, H-18), 7.82–7.78 (m, 2H; H-9, H-11), 7.64–7.61 (m, 4H; TBDPS-aryl-H_{ortho}), 7.43–7.30 (m, 6H; TBDPS-aryl-H_{meta}, -H_{para}), 7.12–7.07 (m, 2H; H-8, H-12), 6.99–6.96 (m, 2H; H-15, H-17), 5.58 (d, $^3J_{1,2} = 1.3$ Hz, 1H; H-1), 4.15 (s, 1H; H-2), 4.08 (dd, $^3J_{2,3} = 2.9$ Hz, $^3J_{3,4} = 9.3$ Hz, 1H; H-3), 4.04–3.96 (m, 3H; H-4, H-19), 3.90 (d, $^3J_{6,5} = 4.9$ Hz, 2H; H-6), 3.71 (ddd ≈ dt, $^3J_{5,6} = 5.0$ Hz, $^3J_{4,5} = 9.8$ Hz, 1H; H-5), 3.14 (s, 1H; O*H*), 3.07 (s, 1H; O*H*), 3.07 (s, 1H; O*H*), 2.81 (s, 1H; O*H*), 2.73–2.70 (m, 2H; H-24), 1.86–1.81 (m, 2H; H-20), 1.77–1.72 (m, 2H; H-23), 1.68 (s, 1H; S*H*), 1.54–1.48 (m, 4H; H-21, H-22), 1.03 ppm (s, 3H; C(CH_3)$_3$); ^{13}C NMR (126 MHz, $CDCl_3$): $\delta = 161.3$ (C-16), 157.7 (C-7), 148.2 (C-13), 146.9 (C-10), 135.6 (TBDPS-aryl-C_{ortho}), 135.5 (TBDPS-aryl-C_{ortho}), 132.7 (TBDPS-aryl-C_{ipso}), 132.7 (TBDPS-aryl-C_{ipso}), 130.0 (TBDPS-aryl-C_{para}), 127.8 (TBDPS-aryl-C_{meta}), 127.8 (TBDPS-aryl-C_{para}), 124.5 (C-14, C-18), 124.2 (C-9, C-11), 116.6 (C-15, C-17), 114.7 (C-8, C-12), 97.6 (C-1), 71.5 (C-5), 71.4 (C-3), 70.1 (C-2), 70.0 (C-4), 68.1 (C-19), 64.8 (C-6), 39.0 (C-24), 29.1 (C-20), 29.1 (C-23), 28.2 (C-22), 26.8 (C(CH_3)$_3$), 25.7 (C-21), 19.2 ppm (C(CH_3)$_3$); MS (ESI): *m*/*z*: calcd for $C_{40}H_{50}N_2O_7SSi$: 730.3125 [*M*]; found: 730.3097; UV/Vis: ε (ethyl acetate) = 19235 ± 74.4 L mol^{-1} cm^{-1}.

(*E*)-*p*-[*p*′-(*N*,*N*-Dimethyl-*S*-thiocarbamoyl)phenylazo]biphenyl 2,3,4,6-tetra-*O*-acetyl-α-D-mannopyranoside (13): The boronic ester **12** (100 mg, 243 μmol), iodoazobenzene **9**, potassium carbonate (102 mg, 738 μmol), and TBABr were dissolved in water/toluene (1:2.5, 14 mL). The mixture was degassed, a catalytic amount of tetrakis(triphenylphosphine)palladium(0) was added, and the resulting mixture was stirred at 80 °C for 4 h and then at room temperature overnight. It was then diluted with ethyl acetate (30 mL) and brine (20 mL). The organic phase was dried over $MgSO_4$, filtered, and concentrated under reduced pressure. Column chromatography (cyclohexane/ethyl acetate, 2:1) gave the desired product as an orange solid (43.1 mg, 60.9 μmol, 25%). $R_f = 0.27$ (cyclohexane/ethyl acetate, 1:1); m.p. 182 °C; $[\alpha]_D^{20} = +61.3$ ($c = 0.91$, CH_2Cl_2); ^{1}H NMR (500 MHz, $CDCl_3$): $\delta = 8.0–7.98$ (m, 2H; H-14, H-18), 7.96–7.93 (m, 2H; H-15, H-17), 7.71–7.69 (m, 2H; H-20, H-24), 7.67–7.60 (m, 4H; H-9, H-11, H-21, H-23), 7.21–7.18 (m, 2H; H-8, H-12), 5.61–5.59 (m, 2H; H-1, H-3), 5.49 (dd, $^3J_{1,2} = 1.8$ Hz, $^3J_{2,3} = 3.5$ Hz, 1H; H-2), 5.40 (dd ≈ t, $^3J_{3,4} = {}^3J_{4,5} = 10.0$ Hz, 1H; H-4), 4.31 (dd, $^3J_{5,6a} = 5.0$ Hz, $^2J_{6a,6b} = 12.0$ Hz, 1H; H-6a), 3.61 (dd, $^3J_{5,6b} = 1.8$ Hz, $^2J_{6a,6b} = 10.9$ Hz, 1H; H-6b), 4.15–4.09 (m, 2H; H-5, H-6b), 3.12, 3.06 (each s, each 3H; 2CH_3), 2.22, 2.07, 2.05, 2.05 ppm (each s, each 3H; 4OAc); ^{13}C NMR (126 MHz, $CDCl_3$): $\delta = 170.5$, 170.0, 170.0, 169.7 (4*C*OCH$_3$), 166.2 (S*C*O), 155.6 (C-7), 152.7 (C-10), 151.6 (C-13), 143.1 (C-16), 136.1 (C-21, C-23), 131.5 (C-19), 131.2 (C-22), 128.4 (C-9, C-11), 127.4 (C-20, C-24), 123.6 (C-14, C-18), 123.1 (C-15, C-17), 116.9 (C-8, C-12), 95.8 (C-1), 69.4 (C-2), 69.3 (C-5), 68.9 (C-3), 65.9 (C-4), 62.1 (C-6), 37.0 (CH_3), 20.9, 20.7, 20.7, 20.7 ppm (4COCH_3); IR (ATR): $\tilde{\nu} = 2937$, 1745, 1214, 1034, 826 cm^{-1}; MS (ESI): *m*/*z*: calcd for $C_{35}H_{37}O_{11}N_3S$+Na$^+$: 703.2041 [*M*]; found: 730.2026; elemental analysis calcd (%) for $C_{35}H_{37}O_{11}N_3S$: C 59.40, H 5.27, N 5.94, S 4.53; found: C 58.57, H 4.90, N 6.21, S 4.75.

(*E*)-*p*-(*p*′-Mercaptophenylazo)biphenyl-α-D-mannopyranoside (14): The thiocarbamate **13** (16.7 mg, 23.5 μmol) was suspended in methanol (1 mL) and potassium hydroxide solution (0.2 mL, 4.3 M in MeOH) was added. The reaction mixture was stirred for 1 h. A second portion of potassium hydroxide solution (0.2 mL, 4.3 M in MeOH) was then added, and the reaction mixture was stirred for 16 h at room temperature. It was then neutralized with 2 M HCl and concentrated under reduced pressure. Potassium chloride was precipitated by the addition of acetone and filtered off. The solvent was removed under reduced pressure and the product was obtained as an orange solid (7.3 mg, 68%). $[\alpha]_D^{20} = +29.3$ ($c = 0.02$, MeOH); ^{1}H NMR (500 MHz, [D$_6$]DMSO): $\delta = 7.88–7.94$ (m, 4H; H-15, H-17, H-20, H-24), 7.88–7.87 (m, 2H; H-15, H-17), 7.81–7.79 (m, 2H; H-21, H-23), 7.74–7.72 (m, 2H; H-9, H-11), 7.22–7.12 (m, 2H; H-8, H-12), 5.47 (d, $^3J_{1,2} = 1.3$ Hz, 1H; H-1), 3.87 (m, 1H; H-3), 3.71 ppm (m, 1H; H-2); ^{13}C NMR (126 MHz, [D$_6$]DMSO): $\delta = 156.5$ (C-10), 151.1 (C-22), 150.5 (C-13), 142.7 (C-16), 138.9 (C-19), 132.3 (C-7), 127.9 (C-9, C-11), 127.6 (C-21, C-23), 127.0 (C-14, C-18), 123.5 (C-20, C-24), 123.2 (C-15, C-17), 117.1 (C-8, C-12), 98.6 (C-1), 74.9 (C-5), 70.5 (C-3), 69.9 (C-2), 66.5 (C-4), 60.0 ppm (C-6); IR (ATR): $\tilde{\nu} = 1589$, 1131, 1001, 825, 557 cm^{-1}; MS (ESI): *m*/*z*: calcd for $C_{24}H_{34}O_6N_2S$+H$^+$: 469.1428 [*M*]; found: 469.1423; UV/Vis: ε (DMSO) = 3756.39 ± 36.0 L mol^{-1} cm^{-1}.

(*E*)-*p*-[*p*′-(*N*,*N*-Dimethyl-*S*-thiocarbamoyl)biphenylazo]phenyl 2,3,4,6-tetra-*O*-acetyl-α-D-mannopyranoside (18): Boronic ester **17** (23.6 mg, 36.1 μmol), thiocarbamate **15** (10.0 mg, 30.5 μmol), potassium carbonate (4.8 mg, 61.0 μmol), and TBABr (5.0 mg, 15.5 μmol) were dissolved in toluene/H_2O (2:1, 6 mL) and the mixture was degassed. A catalytic amount of tetrakis(triphenylphosphine)palladium(0) was then added, and the reaction mixture was stirred at 80 °C for 4 h and for 16 h at room temperature. The phases were allowed to separate, and the organic phase was washed with water (10 mL) and dried over $MgSO_4$. It was then filtered, the solvent was removed under reduced pressure, and the residue was purified by column chromatography (cyclohexane/ethyl acetate, 1:1). The product was obtained as an orange solid (10.3 mg, 14.6 μmol, 48%). $R_f = 0.35$ (cyclohexane/ethyl acetate, 1:1); m.p. 182 °C; $[\alpha]_D^{20} = +85.6$ ($c = 0.15$, CH_2Cl_2); ^{1}H NMR (500 MHz, $CDCl_3$): $\delta = 7.99–7.92$ (m, 4H; H-9, H-11, H-14, H-18), 7.75–7.51 (m, 6H; H-15, H-17, H-20, H-21, H-23, H-24), 7.26–7.20 (m, 2H; H-8, H-12), 5.61 (m, 2H; H-1, H-3), 5.49 (dd, $^3J_{1,2} = 1.8$ Hz, $^3J_{2,3} = 3.4$ Hz, 1H; H-2), 5.40 (dd ≈ t, $^3J_{3,4} = {}^3J_{4,5} = 9.8$ Hz, 1H; H-4), 4.33 (m, 1H; H-6a), 4.15–4.05 (m, 2H; H-5, H-6b), 3.09 (s, 6H; 2CH_3), 2.22, 2.06, 2.05, 2.04 ppm (each s, each 3H; 4OAc); ^{13}C NMR (126 MHz, $CDCl_3$): $\delta = 170.5$, 170.0, 170.0, 196.7 (4*C*OCH$_3$), 166.8 (S*C*O), 157.6 (C-7), 151.9 (C-13), 148.5 (C-10), 142.7 (C-16), 141.1 (C-19), 136.3 (C-22), 136.1 (C-21, C-23), 127.9 (C-15, C-17), 127.7 (C-20, C-24), 123.9 (C-14, C-18), 95.7 (C-1), 69.4 (C-5), 69.3 (C-2), 68.8 (C-3), 65.9 (C-4), 62.1 (C-6), 37.0 (2CH_3), 20.9, 20.7, 20.7, 20.7 ppm (4COCH_3); IR (ATR): $\tilde{\nu} = 1746$, 1365, 1211, 1030, 819 cm^{-1}; MS (ESI): *m*/*z*: calcd for $C_{35}H_{38}O_{11}N_3S$: 708.2222 [*M*]; found: 708.2223.

(*E*)-*p*-[*p*′-(*N*,*N*-Dimethyl-*S*-thiocarbamoyl)biphenylazo]phenyl 2,3,4,6-tetra-*O*-allyl-α-D-mannopyranoside (19): Boronic ester **17** (241 mg, 373 μmol), thiocarbamate **15** (247 mg, 804 μmol), cesium carbonate (237 mg, 727 μmol), and TBABr (25 mg, 78 μmol) were dissolved in toluene/H_2O (10:1, 6 mL). The solution was degassed and tetrakis(triphenylphosphine)palladium(0) (57 mg, 49 μmol) was added. The reaction mixture was stirred at 90 °C for 16 h, diluted with ethyl acetate (30 mL), and washed with 2 M aqueous HCl (20 mL). The organic phase was dried over $MgSO_4$, filtered, and concentrated under reduced pressure. Column chromatography (cyclohexane/ethyl acetate, 4:1) gave the product as an orange oil (70 mg, 100 μmol, 27%). $R_f = 0.05$ (cyclohexane/ethyl acetate, 2:1); $[\alpha]_D^{20} = +95.0$ ($c = 0.10$, CH_2Cl_2); ^{1}H NMR (600 MHz, $CDCl_3$): $\delta =$ 7.97–7.90 (m, 4H; H-9, H-11, H-14, H-18), 7.74–7.72 (m, 2H; H-16, H-17), 7.68–7.66 (m, 2H; H-20, H-24), 7.60–7.58 (m, 2H; H-21, H-23),

7.21–7.18 (m, 2H; H-8, H-12), 6.04–5.85 (m, 4H; *H*C=CH$_2$), 5.65 (d, $^3J_{1,2}$ = 1.5 Hz, 1H; H-1), 5.40–5.22 (m, 6H; 3HC=C*H*$_2$), 5.16–5.12 (m, 2H; HC=C*H*$_2$), 4.38 (ddt, $^4J_{OCH2,CH=CH2}$ = 1.3 Hz, $^3J_{OCH2,CH=CH2}$ = 5.7 Hz, $^2J_{OCHa,OCHb}$ = 12.3 Hz, 1H; OC*H*), 4.29–4.21 (m, 4H; 2OC*H*$_2$), 4.13 (m, 1H; OC*H*), 4.08 (m, 1H; OC*H*), 3.97–3.87 (m, 4H; H-2, H-3, H-4, OC*H*), 3.73 (m, 1H; H-5), 3.69 (dd, $^3J_{5,6a}$ = 4.3 Hz, $^2J_{6a,6b}$ = 10.9 Hz, 1H; H-6a), 3.61 (dd, $^3J_{5,6b}$ = 1.8 Hz, $^2J_{6a,6b}$ = 10.9 Hz, 1H; H-6b), 3.13, 3.06 ppm (each s, each 3H; C*H*$_3$); ^{13}C NMR (150 MHz, $CDCl_3$): δ = 166.8 (SCO), 158.5 (C-7), 152.0 (C-13), 148.0 (C-10), 142.5 (C-22), 141.1 (C-16), 136.3 (C-19), 135.0, 134.9, 134.8, 134.7 (H*C*=CH$_2$), 127.9 (C-15, C-17), 127.6 (C-21, C-32), 124.6 (C-14, C-18), 123.3 (C-9, C-11), 117.8 (OCH$_2$CH=CH$_2$), 116.9 (OCH$_2$CH=CH$_2$), 116.8 (OCH$_2$CH=CH$_2$), 116.7 (C-8, C-12), 116.6 (OCH$_2$CH=CH$_2$), 96.5 (C-1), 79.1 (C-2), 74.5 (C-3), 74.4 (C-4), 74.0 (OCH$_2$CH=CH$_2$), 72.4 (C-5), 72.4 (OCH$_2$CH=CH$_2$), 72.3 (OCH$_2$CH=CH$_2$), 71.4 (OCH$_2$CH=CH$_2$), 68.7 (C-6), 37.0 ppm (2C*H*$_3$); IR (ATR): $\tilde{\nu}$ = 2920, 2853, 1668, 1233, 1130, 1088, 987 cm^{-1}; MS (ESI): *m/z*: calcd for $C_{39}H_{45}O_7N_3S$+Na$^+$: 722.2870 [*M*]; found: 722.2857.

(*E*)-*p*-(*p*′-Mercaptobiphenylazo)phenyl α-D-mannopyranoside (20): The carbamate **18** (37 mg, 55 μmol) and potassium hydroxide (115 mg, 2.03 mmol) were dissolved in methanol. The mixture was degassed with the aid of ultrasound for 10 min and then stirred at 80 °C for 2 h. It was then neutralized with 2 N HCl and concentrated under reduced pressure. The residue was taken up in acetone and filtered to remove precipitated potassium chloride. After removal of the solvent, the product was obtained as an orange amorphous solid (16.5 mg, 35 μmol). $[\alpha]_D^{20}$ = +66.7 (*c* = 0.09, DMSO); ^{1}H NMR (500 MHz, [D$_6$]DMSO): δ = 7.91–7.87 (m, 6H; H-9, H-11, H-14, H-18, H-15, H-17), 7.85–7.81 (m, 2H; H-20, H-24), 7.71–7.69 (m, 2H; H-21, H-23), 7.29–7.27 (m, 2H; H-8, H-12), 5.55 (d, $^3J_{1,2}$ = 1.4 Hz, 1H; H-1), 5.10 (m, 1H; O*H*), 4.86 (m, 1H; O*H*), 4.80 (m, 1H; O*H*), 4.46 (m, 1H; O*H*), 3.87 (m, 1H; H-3), 3.70 (m; H-2), 3.60 (m, 1H; H-6a), 3.52–3.50 ppm (m, 2H; H-4, H-6b); ^{13}C NMR (500 MHz, [D$_6$]DMSO): δ = 158.9 (C-13), 151.2 (C-10), 146.8 (C-7), 141.2 (C-16), 138.2 (C-22), 135.5 (C-19), 127.8 (C-20, C-24), 127.7 (C-21, C-23), 127.4 (C-15, C-17), 124.3 (C-9, C-11), 122.9 (C-14, C-18), 117.02 (C-8, C-12), 98.5 (C-1), 75.2 (C-5), 70.4 (C-3), 69.7 (C-2), 66.6 (C-4), 60.9 ppm (C-6); IR (ATR): $\tilde{\nu}$ = 3249, 2923, 1589, 1131, 1006, 2848, 557 cm^{-1}; MS (ESI): *m/z*: calcd for $C_{24}H_{24}O_6N_2S$: 468.1355 [*M*]; found: 468.1353; UV/Vis: ε (DMSO) = 17631.11 ± 302.48 L mol^{-1} cm^{-1}.

(*E*)-*p*-(*p*′-Mercaptobiphenylazo)phenyl 2,3,4,6-tetra-*O*-allyl-α-D-mannopyranoside (21): The carbamate **19** (26.2 mg, 37.4 μmol) and potassium hydroxide (106 mg, 188 mmol) were dissolved in methanol (2 mL) and the reaction mixture was degassed with the aid of ultrasound for 10 min. It was then stirred for 1 h at 65 °C for 16 h at room temperature. Thereafter, it was neutralized with Amberlite IR120 ion-exchange resin, the resin was filtered off, and the filtrate was concentrated under reduced pressure. The product was obtained as a dark-orange syrup (11.6 mg, 18.4 μmol, 48%). $[\alpha]_D^{20}$ = +97.1 (*c* = 0.07, CH_2Cl_2); ^{1}H NMR (600 MHz, $CDCl_3$): δ = 7.97–7.91 (m, 4H; H-9, H-11, H-14, H-18), 7.74–7.72 (m, 2H; H-16, H-17), 7.68–7.66 (m, 2H; H-20, H-24), 7.60–7.58 (m, 2H; H-21, H-23), 7.21–7.19 (m, 2H; H-8, H-12), 6.04–5.85 (m, 4H; *H*C=CH$_2$), 5.65 (d, $^3J_{1,2}$ = 1.5 Hz, 1H; H-1), 5.40–5.22 (m, 6H; 3HC=C*H*$_2$), 5.16–5.12 (m, 2H; HC=C*H*$_2$), 4.38 (ddt, $^4J_{OCH2,CH=CH2}$ = 1.3 Hz, $^3J_{OCH2,CH=CH2}$ = 5.7 Hz, $^2J_{OCHa,OCHb}$ = 12.3 Hz, 1H; OC*H*), 4.29–4.21 (m, 4H; 2OC*H*$_2$), 4.13 (m, 1H; OC*H*), 4.08 (m, 1H; OC*H*), 3.97–3.87 (m, 4H; H-2, H-3, H-4, OC*H*), 3.73 (m, 1H; H-5), 3.69 (dd, $^3J_{5,6a}$ = 4.3 Hz, $^2J_{6a,6b}$ = 10.9 Hz, 1H; H-6a), 3.61 (dd, $^3J_{5,6b}$ = 1.8 Hz, $^2J_{6a,6b}$ = 10.9 Hz, 1H; H-6b), 3.52 ppm (s, 1H; S*H*); ^{13}C NMR (150 MHz, $CDCl_3$): δ = 158.6 (C-7), 152.0 (C-13), 148.0 (C-10), 135.0, 135.0, 134.9, 134.7 (H*C*=CH$_2$), 131.0 (C-23), 129.8 (C-21), 128.2 (C-24), 127.8 (C-20), 127.8 (C-16), 127.7 (C-19), 127.6 (C-15, C-17), 127.4 (C-22), 124.7 (C-14, C-18), 123.3 (C-9, C-11), 117.8 (OCH$_2$CH=CH$_2$), 116.9 (OCH$_2$CH=CH$_2$), 116.8 (OCH$_2$CH=CH$_2$), 116.7 (C-8, C-12), 116. 6 (OCH$_2$CH=CH$_2$), 96.5 (C-1), 79.2 (C-2), 74.5 (C-3), 74.4 (C-4), 74.0 (OCH$_2$CH=CH$_2$), 72.4 (C-5), 72.4 (OCH$_2$CH=CH$_2$), 72.3 (OCH$_2$CH=CH$_2$), 71.4 (OCH$_2$CH=CH$_2$), 68.7 ppm (C-6); IR (ATR): $\tilde{\nu}$ = 2921, 2856, 1597, 1497, 1233, 1130, 1102, 986 cm^{-1}; MS (ESI): *m/z*: calcd for $C_{36}H_{40}O_6N_2S$+Na$^+$: 722.2870 [*M*]; found: 722.2857; UV/Vis: ε ($CHCl_3$) = 26549.98 ± 298.19 L mol^{-1} cm^{-1}.

Acknowledgements

We thank the Deutsche Forschungsgemeinschaft for financial support of projects B11, C01, and C11 within SFB 677. Furthermore, we would like to thank the Helmholtz-Zentrum Berlin for providing the beamtime at the HE-SGM beamline (XPS and NEXAFS measurements) and Prof. Christof Wöll (KIT) for providing the Prevac endstation with support by Dr. Alexei Nefedov (also KIT).

Conflict of interest

The authors declare no conflict of interest.

Keywords: azobenzenes · glyco-SAMs · monolayers · photochemistry · photoswitchable carbohydrate orientation

[1] *Essentials of Glycobiology* (Eds.: A. Varki, R. D. Cummings, J. D. Esko, P. Stanley, G. W. Hart, M. Aebi, A. G. Darvill, T. Kinoshita, N. H. Packer, J. H. Prestegard, R. L. Schnaar, P. H. Seeberger), Cold Spring Harbor Laboratory Press, New York, **2017**.

[2] M. Ambrosi, N. R. Cameron, B. G. Davis, *Org. Biomol. Chem.* **2005**, *3*, 1593 – 1608.

[3] P. Chahales, D. G. Thanassi, *Microbiol. Spec.* **2015**, *3*, https://doi.org/10.1128/microbiolspec.UTI-0018-2013.

[4] J. Poole, C. J. Day, M. v. Itzstein, J. C. Paton, M. P. Jennings, *Nat. Rev. Microbiol.* **2018**, *16*, 440 – 452.

[5] a) N. Laurent, J. Voglmeir, S. L. Flitsch, *Chem. Commun.* **2008**, *37*, 4400 – 4412; b) L. Ban, M. Mrksich, *Angew. Chem. Int. Ed.* **2008**, *47*, 3396 – 3399; *Angew. Chem.* **2008**, *120*, 3444 – 3447; c) Y. Liu, A. S. Palma, T. Feizi, *Biol. Chem.* **2009**, *390*, 647 – 656; d) P. M. Dietrich, T. Horlacher, P.-L. Girard-Lauriault, T. Gross, A. Lippitz, H. Min, T. Wirth, R. Castelli, P. H. Seeberger, W. E. S. Unger, *Langmuir* **2011**, *27*, 4808 – 4815; e) C. Grabosch, M. Kind, Y. Gies, F. Schweighöfer, A. Terfort, T. K. Lindhorst, *Org. Biomol. Chem.* **2013**, *11*, 4006 – 4015; f) J. K. Bhattarai, D. Neupane, V. Mikhaylov, A. V. Demchenko, K. J. Stine, in *Carbohydrate* (Eds.: M. Caliskan, I. H. Kavakli, G. C. Oz), IntechOpen **2017**, 63; g) Z.-L. Zhi, N. Laurent, A. K. Powell, R. Karamanska, M. Fais, J. Voglmeir, A. Wright, J. M. Blackburn, P. R. Crocker, D. A. Russell, S. Flitsch, R. A. Field, J. E. Turnbull, *ChemBioChem* **2008**, *9*, 1568 – 1575; h) I. Tavernaro, S. Hartmann, L. Sommer, H. Hausmann, C. Rohner, M. Ruehl, A. Hoffmann-Roeder, S. Schlecht, *Org. Biomol. Chem.* **2015**, *13*, 81 – 97.

[6] V. Chandrasekaran, H. Jacob, F. Petersen, K. Kathirvel, F. Tuczek, T. K. Lindhorst, *Chem. Eur. J.* **2014**, *20*, 8744 – 8752.

[7] T. Weber, V. Chandrasekaran, I. Stamer, M. B. Thygesen, A. Terfort, T. K. Lindhorst, *Angew. Chem. Int. Ed.* **2014**, *53*, 14583 – 14586; *Angew. Chem.* **2014**, *126*, 14812 – 14815.

[8] a) L. Möckl, A. Müller, C. Bräuchle, T. K. Lindhorst, *Chem. Commun.* **2016**, *52*, 1254 – 1257; b) G. Despras, L. Möckl, A. Heitmann, I. Stamer, C. Bräuchle, T. Lindhorst, *ChemBioChem* **2019**, *20*, 2373 – 2382.

[9] J. C. Love, L. A. Estroff, J. K. Kriebel, R. G. Nuzzo, G. M. Whitesides, *Chem. Rev.* **2005**, *105*, 1103 – 1169.

[10] R. Klajn, *Pure Appl. Chem.* **2010**, *82*, 2247 – 2279.

[11] W. R. Browne, B. L. Feringa, *Annu. Rev. Phys. Chem.* **2009**, *60*, 407 – 428.

[12] J. Zhang, J. K. Whitesell, M. A. Fox, *Chem. Mater.* **2001**, *13*, 2323 – 2331.
[13] a) B. Baisch, D. Raffa, U. Jung, O. M. Magnussen, C. Nicolas, J. Lacour, J. Kubitschke, R. Herges, *J. Am. Chem. Soc.* **2009**, *131*, 442 – 443; b) U. Jung, C. Schütt, O. Filinova, J. Kubitschke, R. Herges, O. Magnussen, *J. Phys. Chem. C* **2012**, *116*, 25943 – 25948; c) A. Schlimm, R. Löw, T. Rusch, F. Röhricht, T. Strunskus, T. Tellkamp, F. Sönnichsen, U. Manthe, O. Magnussen, F. Tuczek, R. Herges, *Angew. Chem. Int. Ed.* **2019**, *58*, 6574 – 6578; *Angew. Chem.* **2019**, *131*, 6646 – 6650.
[14] H. Jacob, S. Ulrich, U. Jung, S. Lemke, T. Rusch, C. Schütt, F. Petersen, T. Strunskus, O. Magnussen, R. Herges, F. Tuczek, *Phys. Chem. Chem. Phys.* **2014**, *16*, 22643 – 22650.
[15] J. Lahann, S. Mitragotri, T.-N. Tran, H. Kaido, J. Sundaram, I. S. Choi, S. Hoffer, G. A. Somorjai, R. Langer, *Science* **2003**, *299*, 371 – 374.
[16] G. Pace, V. Ferri, C. Grave, M. Elbing, C. von Hänisch, M. Zharnikov, M. Mayor, M. A. Rampi, P. Samorì, *Proc. Natl. Acad. Sci. USA* **2007**, *104*, 9937 – 9942.
[17] J. Zhang, P. Kovac, *J. Carbohydr. Chem.* **1999**, *18*, 461 – 469.
[18] J. K. Fairweather, T. Karoli, V. Ferro, *Bioorg. Med. Chem.* **2004**, *12*, 6063 – 6075.
[19] V. Chandrasekaran, E. Johannes, H. Kobarg, F. D. Sönnichsen, T. K. Lindhorst, *ChemistryOpen* **2014**, *3*, 99 – 108.
[20] N. Miyaura, A. Suzuki, *Chem. Rev.* **1995**, *95*, 2457 – 2483.
[21] Z. Han, J. S. Pinkner, B. Ford, E. Chorell, J. M. Crowley, C. K. Cusumano, S. Campbell, J. P. Henderson, S. J. Hultgren, J. W. Janetka, *J. Med. Chem.* **2012**, *55*, 3945 – 3959.
[22] A. Perjessy, R. G. Jones, S. L. McClair, J. M. Wilkins, *J. Org. Chem.* **1983**, *48*, 1266 – 1271.
[23] J. M. Chalker, C. S. C. Wood, B. G. Davis, *J. Am. Chem. Soc.* **2009**, *131*, 16346 – 16347.
[24] C. Kallweit, G. Haberhauer, S. Woitschetzki, *Chem. Eur. J.* **2014**, *20*, 6358 – 6365.
[25] a) J. Strueben, M. Lipfert, J.-O. Springer, C. A. Gould, P. J. Gates, F. D. Sönnichsen, A. Staubitz, *Chem. Eur. J.* **2015**, *21*, 11165 – 11173; b) A. Moanta, *J. Chil. Chem. Soc.* **2014**, *59*, 2275 – 2278.
[26] U. Jung, S. Kuhn, U. Cornelissen, F. Tuczek, T. Strunskus, V. Zaporojtchenko, J. Kubitschke, R. Herges, O. Magnussen, *Langmuir* **2011**, *27*, 5899 – 5908.
[27] S. Ulrich, U. Jung, T. Strunskus, C. Schütt, A. Bloedorn, S. Lemke, E. Ludwig, L. Kipp, F. Faupel, O. Magnussen, R. Herges, *Phys. Chem. Chem. Phys.* **2015**, *17*, 17053 – 17062.
[28] H. Jacob, K. Kathirvel, F. Petersen, T. Strunskus, A. Bannwarth, S. Meyer, F. Tuczek, *Langmuir* **2013**, *29*, 8534 – 8543.
[29] L. Hallmann, A. Bashir, T. Strunskus, R. Adelung, V. Staemmler, C. Wöll, F. Tuczek, *Langmuir* **2008**, *24*, 5726 – 5733.
[30] H. Wackerbarth, R. Marie, M. Grubb, J. Zhang, A. G. Hansen, I. Chorkendorff, C. B. V. Christensen, A. Boisen, J. Ulstrup, *J. Solid State Electrochem.* **2004**, *8*, 474 – 481.
[31] a) R. G. Nuzzo, F. A. Fusco, D. L. Allara, *J. Am. Chem. Soc.* **1987**, *109*, 2358 – 2368; b) Z. Hou, S. Dante, N. L. Abbott, P. Stroeve, *Langmuir* **1999**, *15*, 3011 – 3014; c) M. D. Porter, T. B. Bright, D. L. Allara, C. E. D. Chidsey, *J. Am. Chem. Soc.* **1987**, *109*, 3559 – 3568; d) L. H. Dubois, R. G. Nuzzo, *Annu. Rev. Phys. Chem.* **1992**, *43*, 437 – 463.
[32] R. G. Greenler, *J. Chem. Phys.* **1966**, *44*, 310 – 315.
[33] a) A. Cembran, F. Bernardi, M. Garavelli, L. Gagliardi, G. Orlandi, *J. Am. Chem. Soc.* **2004**, *126*, 3234 – 3243; b) A. R. A. Mostad, *Acta Chem. Scand.* **1971**, *25*, 3561 – 3568.
[34] a) A. Turchanin, D. Käfer, M. El-Desawy, C. Wöll, G. Witte, A. Gölzhäuser, *Langmuir* **2009**, *25*, 7342 – 7352; b) W. Geyer, V. Stadler, W. Eck, M. Zharnikov, A. Gölzhäuser, M. Grunze, *Appl. Phys. Lett.* **1999**, *75*, 2401 – 2403; c) S. Frey, H.-T. Rong, K. Heister, Y.-J. Yang, M. Buck, M. Zharnikov, *Langmuir* **2002**, *18*, 3142 – 3150; d) A. Shaporenko, K. Rössler, H. Lang, M. Zharnikov, *J. Phys. Chem. B* **2006**, *110*, 24621 – 24628; e) W. Azzam, B. I. Wehner, R. A. Fischer, A. Terfort, C. Wöll, *Langmuir* **2002**, *18*, 7766 – 7769; f) P. Cyganik, M. Buck, T. Strunskus, A. Shaporenko, J. Wilton Ely, M. Zharnikov, C. Wöll, *J. Am. Chem. Soc.* **2004**, *126*, 5960 – 5961.
[35] A. E. McDermott, T. Polenova, *Solid State NMR Studies of Biopolymers*, Wiley, **2012**.
[36] J. Stöhr, D. A. Outka, *Phys. Rev. B* **1987**, *36*, 7891 – 7905.

Manuscript received: August 9, 2019
Revised manuscript received: October 21, 2019
Accepted manuscript online: October 29, 2019
Version of record online: December 10, 2019

